ENERGY BALANCE MODELS WITH THREE PHASES OF WATER FEEDBACK

SIMON FULLICK

MASTER OF SCIENCE THESIS

UC
UNIVERSITY OF
CANTERBURY
Te Whare Wānanga o Waitaha
CHRISTCHURCH NEW ZEALAND

DEPARTMENT OF PHYSICS AND ASTRONOMY
UNIVERSITY OF CANTERBURY
PRIVATE BAG 4800, CHRISTCHURCH, NEW ZEALAND

SENIOR SUPERVISOR: ASSOCIATE PROFESSOR ADRIAN MCDONALD

ABSTRACT

Simple one-dimensional heat balance equations have been used to understand climate concepts since the 1960s, when a class of models was developed known as energy balance models (EBMs). EBMs use the growth or loss of polar surface ice as a climatic feedback, giving rise to surprisingly complex non-linear behaviours. One aspect of EBMs that has been relatively poorly examined is the effects of feedbacks caused by the other two phases of water in Earth's climate other than ice: water clouds and water vapour. Cloud and water vapour play a critical role in the energy balance of Earth's climate, and yet are some of the least well understood elements of the global climate system.

This thesis explores the behaviour and interrelationships of climatic feedbacks caused by water in all three phases as it exists in the climate: surface ice caps, water vapour, and liquid water clouds. A two-layered EBM was modified with parameterizations of water vapour and liquid water clouds in order to conduct experiments. Three variants of the model were produced, each with progressively more water feedbacks than the last: a 1 phase model (with only surface ice feedback), a 2 phase model (with surface ice and water vapour) and a 3 phase model (with surface ice, water vapour, and cloud). The models were found to give generally realistic results, but with an underestimation of water vapour density, which in turn reduced the generated cloud fraction in the 3 phase model. Thus, the impacts of these extra feedbacks were likely to be underestimated in the analysis in general.

The sensitivity of the model to several prognostic variables was studied by observing the changes in the model to a range of each variable. The 3 phase model was less sensitive to changes to the solar constant, S_0, which measures incoming solar radiation, than the 1 phase model. This was probably caused by cloud reflecting and absorbing some radiation from the sun that would have otherwise reached the surface, changing the ratio of atmospheric heat transport to surface heat transport from 2.4953 for the 1 phase model to 2.0626 for the 3 phase model. Changing surface and ice albedo values resulted in changes in the model's stability. The model was found to be insensitive to changes in surface humidity that drives the amount of water vapour the system has available, due to underestimation of water vapour in the model.

The stability of the model was examined, and the 1 phase model was found to respond faster to changes in S_0 than the 3 phase model. The model was tested for hysteresis, which was confirmed for all three model variants. The 1 phase model showed less stability then the 3 phase model as S_0 was increased, but both models were similarly stable as S_0 was decreased.

That, if I then had waked after long sleep,
Will make me sleep again. And then, in dreaming,
The clouds methought would open and show
riches
Ready to drop upon me, that when I waked
I cried to dream again.

— Shakespeare, The Tempest

ACKNOWLEDGEMENTS

CONTENTS

LIST OF FIGURES

LIST OF TABLES

INTRODUCTION

Simple one-dimensional heat balance equations have been used to understand climate concepts since Budyko [8] and Sellers' [53] classic 1969 papers, which developed a class of simplistic climate models known as "energy balance models" (EBMs), which act to model the global climate by concentrating only on factors that add, remove, or move heat around the Earth. Both papers detail similar heat balance models that use the growth or loss of polar surface ice as a climatic feedback, giving rise to non-linear solutions of those models. One aspect of EBMs that has been relatively poorly examined is the effects of feedbacks caused by the other two phases of water in Earth's climate other than ice: clouds and water vapour. Cloud and water vapour play a critical role in the energy balance of Earth's climate [23] [50] [44], and yet are some of the least well understood elements of the global climate system. Figure 1 shows two syntheses of empirical climate data from 1997 [31] and 2012 [54]. In the space of 15 years between the two studies, there are significant differences in the values associated with the energy balance, and water-based elements have some of the largest changes (for example the difference in latent heating and reflected solar radiation by cloud and atmosphere values), and these values are critical to the understanding of the base state of energy balance in the climate.

This work aims to extend an EBM to explicitly parameterize cloud and water vapour so that the feedbacks and interactions associated with them can be studied in conjunction with surface ice feedbacks. With this, the interrelationship between all three phases of water that exist on Earth can be better understood.

1.1 COMPONENTS OF THE ENERGY BALANCE OF THE EARTH

1.1.1 *Radiative Processes*

On Earth, the vast majority of energy in the atmosphere comes from the Sun. Since the atmosphere borders on a vacuum, there is no medium to collide with for that energy to be dissipated by kinetic collisions, and neither can it be lost by in any significant amount by the escape of energetically heated particles, as the atmosphere is bound to the surface by gravity. Therefore, the only processes of energy loss
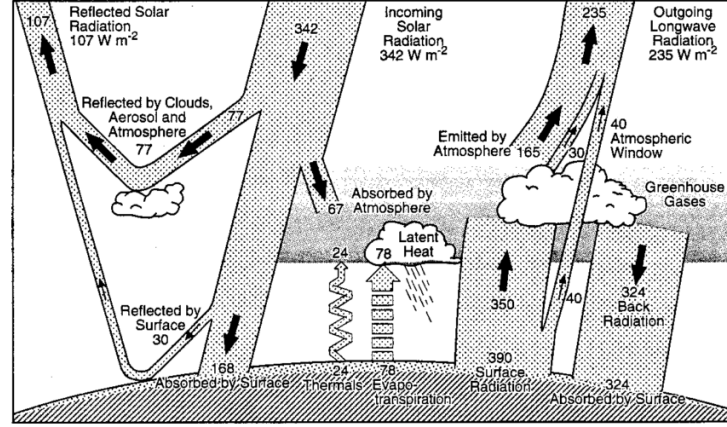
(a) 1997 values (Source: [31])
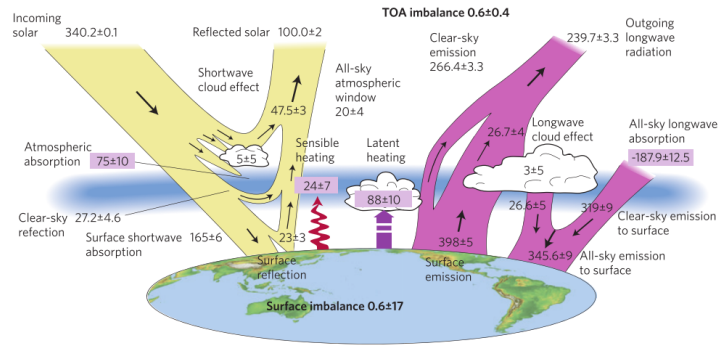
(b) 2012 values (Source: [54])

Figure 1: Comparison of global energy balance values from empirical studies in 1997 and 2012

away from the Earth available is by radiation. Radiative processes can be quantified by principles of blackbody radiation [45].

The cumulative power, F, of an emitting blackbody will be the integral of the Planck function (the energy emitted by a blackbody at a particular wavelength of light) over all wavelengths, which in turn can be simplfied as the Stefan-Boltzmann law:

$$F = \sigma T^4 \tag{1}$$

where σ is the Stefan-Boltzmann constant value, and T is the temperature of the blackbody. This definition of energy flux is for a perfect blackbody, and so must be modified for real objects, which do not emit perfectly. The adjusted value used is known as emissivity, ϵ.

Suppose an object is placed in a cavity kept at a constant temperature. The object is thus illuminated uniformly by blackbody radiation. The *absorptivity* is a measure of the fraction of radiation absorption

per unit of radiation falling on the object, per unit wavelength. Similarly, the *emissivity* is the rate of emission of radiation from the object in all directions as a fraction of the radiation emitted by a perfect blackbody radiator of the same spacial dimensions of the object, per unit wavelength. The wavelength dependence is crucial for understanding the nature of emission and absorption - a good emitter at one wavelength may be a poor one at another. For the purposes of the thesis, it is assumed that the emissivity of an object is its emissivity in the wavelength range of the greatest emission, which for bulk emitters in the atmosphere like cloud and water vapour is largely in the infrared. The absorptivity wavelength bands of interest is both the band emitted by the sun, and the infrared-peaked range of other re-emitters of radiation in the atmosphere itself. *Reflectivity* is the ability of an object to reflect radiation, without absorbing it. Again, good reflectors at certain wavelengths can be poor ones at others, and crucially, good reflectors at certain wavelengths can be poor emitters at those same wavelengths. What this means for modelling energy balance is that the emission and absorption for materials in the atmosphere must be quantified for the wavelength bands of radiation that pass through it - for the purposes of this thesis, this will be two bands (as seen in Figure 2):

- **Shortwave**: a shorter wavelength band from the sun, peaking at approximately 500 nm.

- **Longwave** : a longer wavelength band emitted by the materials in the atmosphere, peaking at approximately 10,000 nm.

A good illustration of the differences between reflectivity and emissivity is the "blanketing effect" of cloud in Earth's atmosphere. Intuitively, we expect to find that a morning after a cloudy night will be warmer (all other things being equal) than a clear night. The explanation normally attributed to this (the reflectiveness of cloud), is incorrect however. The incorrect assumption is that since cloud is highly reflective in visible wavelengths, it must also be so in infrared wavelengths typical of those emitted from the ground [6]. Clouds are almost black in the infrared. What is actually occuring is that cloud is highly emissive in the infrared, compared with water vapour, and this emission causes the heating effect of the atmosphere below the cloud.
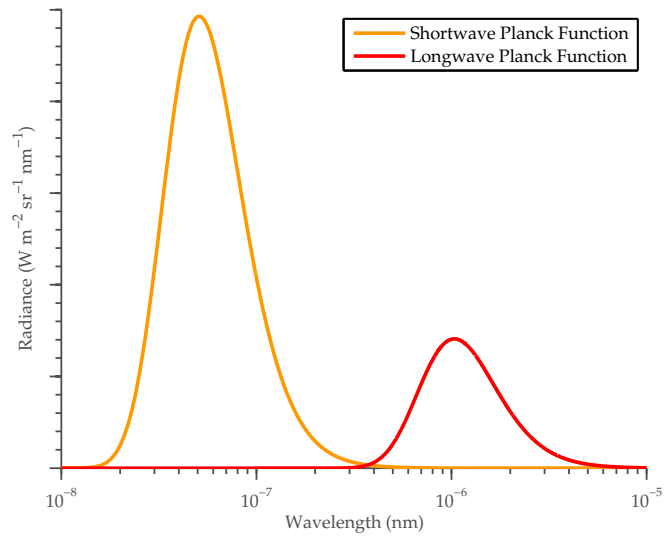
Figure 2: Wavelength bands of emitters. Y axis is not to scale.

1.1.2 *Heat Transport*

Overall, radiative processes described in Section 1.1.1 act to cool high latitudes and warm lower ones. This is due to the uneven mean annual distribution of sunlight across the Earth - incoming shortwave radiation from the sun is on average greater than outgoing longwave radiation at low latitudes, but lower at high latitudes. The component of energy balance in the climate that offsets these processes and brings it into equilibrium is poleward heat transport, transporting the extra heat from the low latitudes to the higher ones [57].

Atmospheric model literature refers to bodily transport of energy by fluid motions as "heat transport". This is not technically accurate, as heat is a quantity of exchange, rather than a property of a fluid [51]. Care should be taken in conceptualizing heat transport, as using this term can confuse it with actual heat flux from radiative processes, which are not the same.

The basis for meridional heat transport in the atmosphere is the fundamental imbalance in net radiation received between equatorial and polar latitudes (Figure 3). This causes a meridional temperature gradient, which is then diffused as heat transport from the equator to the pole. Figure 4 shows this measured as northward heat transport in the climate system. The solid line is the estimated total heat transport in the system in petawatts as a function of latitude, and this is compared to the estimated components of the heat transport from the ocean/surface (dashed) and atmosphere (dot-dashed). The
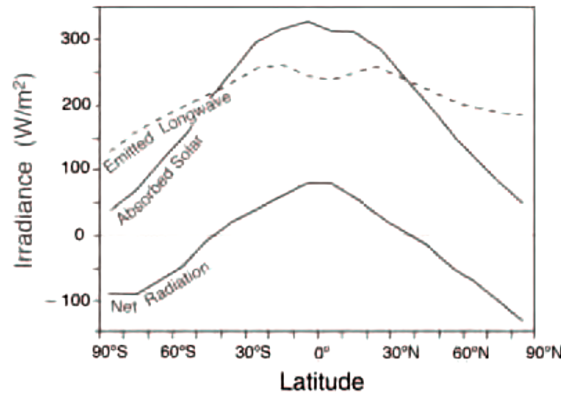
Figure 3: Imbalance in net radiation between equatorial and polar latitudes as a basis for diffusion of heat (Source: [38])
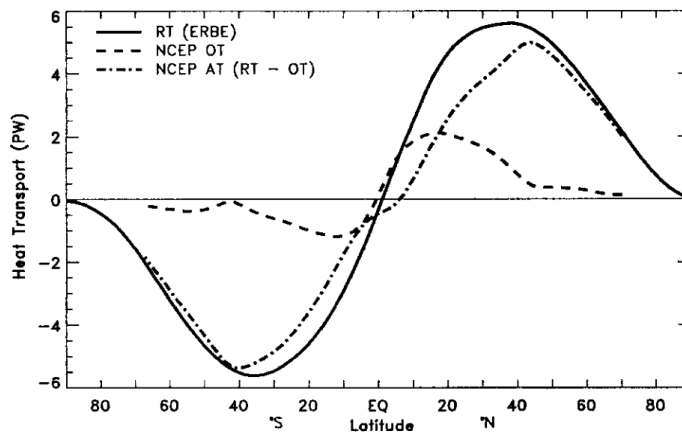
Figure 4: Northward heat transport in climate from NCEP reanalysis data (Source: [57])

estimates were derived from NCEP (ECMWF) reanalysis data. More complex physical processes are also involved in meridional heat transport (Hadley Cells, baroclinic instability, and so on [38]), but lie outside the scope of detail required for models of the complexity dealt with in this thesis.

1.1.3 Convection

One heat transport process in the climate system that has not been mentioned is convection. Convective processes are important to the movement of heat through transport of energetic mass around the atmosphere, but are not modelled by EBMs, as convective processes would add to many parameters, constants, and behaviours to be in

keeping with the simplicity ethos of energy balance models. For this reason convection is not considered in the models used in this thesis.

1.2   MODELLING THE ENERGY BALANCE OF THE EARTH

1.2.1   *Climate Models*

Climate models seek to represent the processes that produce climate, by producing physical, chemical, or and/or biological characterizations of some or all of these processes. These characterizations are described in terms of mathematical equations, with parameters representing various physical aspects of the system. All climate models are neccessarily simplifications of the physical world, and can be characterised into a hierarchy of models, based on the level of complexity in relation to the physical world implemented by them. Loosely speaking, there are three levels to this hierarchy, in order of complexity:

1. Energy Balance Models

2. Earth System Models of Intermediate Complexity

3. General Circulation Models

At the simplest level in the hierarchy, Energy balance models (EBMs) take the physics of radiation transfer (Section 1.1.1), and couple them with bulk heat transport (Section 1.1.2), to give a system to be studied that explicitly conserves only energy, in either zero or one spatial dimensions (the one dimensional EBMs are in terms of latitude). At the most complex level, General Circulation Models (GCMs), are models which conserve energy, mass and momentum. Earth System Models of Intermediate Complexity (EMICs) occupy a position in complexity between these two models, where more interacting components are included (a property sometimes referred to as the "integration" of a model [37]) or dimensions used than EBMs, but with some components parameterized away so that the models can be run more quickly than a more integrated model like a GCM. A possible fourth layer that does not fit this hierarchy as well are radiative-convective models [46], which can and do model very complex levels of behaviour, but generally are only run for a single column of atmosphere.

Simple does not imply less useful, however. While it would be tempting to perceive the increasing complexity of climate models in the hierarchy as a historical progression from simple to complex, EBMs are still used today, and still produce results that are worthwhile. The reason for this is GCMs can be as difficult to study and

quantify as the real climate, and this can often lead to them being treated as "black boxes" - inscrutable objects that must be studied by their output and behaviour, as detailed study of the interaction of their components is difficult. GCMs also require large amounts of computing power, and so are less feasible for studies that require many runs of the model to bear useful results. EBMs, by contrast, are programmatically simple, and so each component of an EBM can be studied in relation to every other component in a way not possible for a GCM, and run many more times with less computing power than a GCM, allowing for broad sensitivity studies of parameters to be carried out. This means that the many differences in the empirical study of Earth's energy balance (like in Figure 1) can be explored efficiently in EBMs first, before GCMs are built to take new studies into account.

A large group of research in EBMs, but not dealt with in this thesis, is paleoclimate research. Paleoclimate research studies geological time scales (up to scales of millions of years) and the behaviour of Earth's climate into the deep past, and the low computing power of EBMs are essential for making modelling millions of years of climate change feasible with current computing power. The snowball and ice free states common to EBMs (which will be covered in Chapter 4) are hypothesized to have occurred in Earth's past [26].

1.2.2 *Water and The Atmosphere*

Water affects the energy balance of the climate system in several ways. In the atmosphere water in a gas phase (vapour), and in a liquid phase (liquid water cloud), have unique effects on radiative processes and heat transport. Water vapour is the largest contribution to the "natural" of the greenhouse effect, and also acts to amplify the greenhouse effect of other gases, for example water vapour feedback doubles the greenhouse warming effect of CO_2 in GCMs [29]. Water vapour is also the principal absorber of incoming shortwave radiation in the troposphere [21].Clouds are very effective absorbers of terrestrial radiation. Clouds become opaque to longwave radiation when their liquid water path (the total amount of liquid water between the top and bottom of the cloud layer) is larger than $20 gm^{-2}$ [21]. Clouds are relatively weak absorbers of solar shortwave, but they are effective scatterers of shortwave, reflecting much solar radiation out to space. The reason for this is that water molecules are far better scatterers when part of a coherent array (like a water droplet in a cloud) than as individual molecules [6].

On top of these effects, there are feedbacks in the climate system associated with both cloud and water vapour. These feedbacks are a major component of existing inter-run variability in GCMs [34] [28]. The amount of water vapour is affected by the temperature of the atmosphere - the maximum partial pressure of water vapour being largely governed by the temperature of the air it resides in (a relation known as the Clausius-Clapeyron relation), and this in turn governs the amount of water vapour available to condense into cloud. Since both water vapour and cloud reflect, absorb, and emit radiation, they can effect the temperature of the atmosphere, creating feedback processes.

1.2.3   *Greenhouse Gases*

One more element of the climate that affects the global energy balance are "greenhouse" gases, such as carbon dioxied (CO_2) and methane (CH_4). These gases act to absorb and emit longwave radiation and act as a net forcing on the heat balance of the climate [20]. Greenhouse gases and their effects on EBMs are not covered in detail in this thesis.

ENERGY BALANCE MODELS: A REVIEW

Energy balance models have been widely used to examine various elements of the climate system. This chapter provides a brief review of EBMs. The early history of EBMs (especially from 1969 to 1981) is relevant due to the plethora of papers produced in that era that cemented the areas and directions of research up to the present day. Additions to the EBM schema are studied, and in particular, a focus is given to EBMs that examine water and how it is represented in various elements of the climate system, as this is relevant to the model created for this thesis.

2.1 EARLY HISTORY OF ENERGY BALANCE MODELS

The first work considering the energy balance of the Earth is generally thought to be Fourier's paper "On the Temperatures of the Terrestrial Sphere and Interplanetary Space" in 1827 [17]. Fourier's work determined that the Earth should be considerably colder than it actually is, if radiation from the Sun is the only heat source. He concluded that there was a possibility that Earth's atmosphere was acting as an insulator, although he mistakenly attributed interstellar radiation as a significant source of heat also. This first formulation of the so-called "greenhouse effect" allowed for further work to determine the actual heat balance budget of the Earth.

The work to determine Earth's heat balance started with W.H. Dines [12], and came to the conclusion that "no appreciable change of temperature occurs from year to year, the actual amount received in one year must be equal to the amount lost", and that "we must be able to write down a set of linear equations between certain of the quantities involved". This approach is essentially that of the energy balance model: an equation with each parameter representing an input or output of heat into or between elements of the Earth-atmosphere system. Dine's system was static with no opportunity for change - concern of a warming planet in the mid-20th century, and insights from paleoclimatology prompted development of a more dynamic model.

The development of contemporary, dynamic EBMs started with Budyko [8] and Sellers [53], who (virtually) simultaneously developed one-dimensional models that incorporated a feedback into the system through the position and movement of ice caps. Annual mean

energy flux at the top of the atmosphere is balanced against meridional diffusion of heat, using temperature differentials as the variable to determine the rate of diffusion, and the formation of ice. Ice forms in the model below some critical temperature, and with reduced incoming flux at the poles (due to ice having a greater albedo than non-ice surfaces), ice caps may form. This class of model is known as the Budyko-Sellers model. The major point of difference between the two models was the treatment of heat diffusion. Budyko simplified heat transport in a linear function [8]:

$$\gamma[T(x) - T_0] \tag{2}$$

Where T_0 is the mean surface temperature, $T(x)$ is the temperature at a given latitude, and γ is a diffusion rate adjustment constant. Sellers used a diffusive term [53]:

$$-\frac{d}{dx}D(1 - x^2)\frac{dT(x)}{dx} \tag{3}$$

Where D is the diffusivity constant, x is the sine of latitude. Whilst Budyko's version was mathematically simple to solve, the Seller's diffusive heat transport term had a direct physical analogue in heat conduction, and therefore would guarantee physically realizable solutions, which Budyko's could not [43].

An analytical solution to the Sellers-style equation set was developed by North [41]. Held and Suarez [24] showed that this analytical solution could also be applied to a Seller-style model with a separate PDE for surface and atmosphere layers, opening up the possibility of examining ocean/surface parameters seperately to atmospheric parameters, and allowing two-layer models to build directly on the early results of one layer Seller-style EBMs. This result is especially relevant to the thesis, as the model developed uses this two-layered approach also.

A review of the work of EBMs up to 1981 can be found in a paper by North [43].

2.2 STABILITY

A distinctive feature of EBMs is their stability behaviour. Stability in EBMs has been extensively studied, both to better understand the model category, and in particular for paleoclimate research in order to better understand the conditions for the onset and end of glaciation periods in Earth's past, and to explore the validity of the so-called

"Snowball Earth" hypothesis. The snowball earth hypothesis states that at some time in Earth's deep past (during the Neoproterozoic era some 700 million years ago), Earth's entire surface was frozen [15]. The Snowball Earth hypothesis is one of a few contested paleo-climate hypotheses for the state of the Earth during Neoproterozoic glaciations. Another hypothesis is the so-called "Slushball Earth" hypothesis [11], which modifies the Snowball Earth by allowing for the coexistence of unfrozen oceans and sea-level glaciers in the tropics. This hypothesis affects the stability criteria of exit from the frozen state, requiring approximately two orders of magnitude less CO_2 than the snowball theory, which means that the Earth possibly stayed in a frozen state for less time than the snowball Earth hypothesis estimates. It also affects stability by requiring more CO_2 to melt back to modern ice levels than the snowball Earth, as the newly exposed ocean would act as a sink for carbonates.

2.2.1 *Small Ice Cap Instability (SICI)*
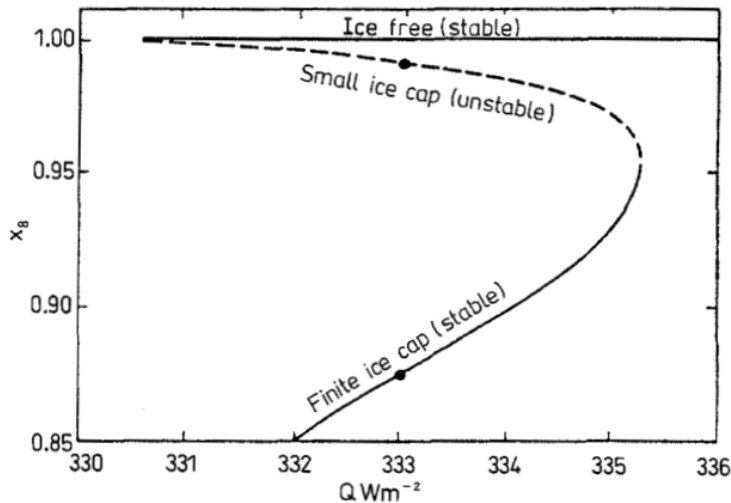
Figure 5: Sine of latitude of equilibrium ice edge x, versus surface solar constant Q (Q is S_0 adjusted for geometrical effects of the Earth). Increasing Q just past $335\,\mathrm{Wm}^{-2}$ causes an abrupt transition to an ice free state. The dotted line represents solutions to the EBM that will always equilibrate in an ice-free state. (Source: [33])

One pervasive feature affecting EBM stability is the small ice edge instability (SICI). Discontinuous albedos at the ice edge have long been known to produce an effect where for small ice caps (less than approximately 20 degrees in extent), the ice edge is unstable and the

model will end in the ice-free solution [8] [53] [41]. This also occurs for ice edges greater than 70 degrees in extent, with the final position being that of a Snowball state solution. Figure 5 shows an EBM near the instability zone - Increasing the solar constant (Q) just past $335 \, \mathrm{Wm}^{-2}$ causes an abrupt transition to an ice free state from a finite ice edge state, with none of the ice edge values in between being stable equilibrium points.

Originally this was thought to be a particular peculiarity of EBMs, and various ad hoc solutions were used to eliminate it, as it was a phenomenon that did not consitently occur in GCMs (although many did exhibit the behaviour in some way) and so was thought to be a mathematical anomaly [9] [42]. Use of ice feedback alone may have oversimplified the understanding of instability in EBMs, however [19]. Lin and North investigated the causes of abrupt state change with land "caps" and seasonal parameterisations, and found the seasonal distribution of insolation and the size and position of land caps had a significant effect on the latitude of onset, and character of SICI behaviour [35]. Lee and North [33] found that SICI behaviour was reduced or removed when they added a small amplitude forcing parameter, but that this was dependent on the magnitude of the forcing.

2.3 ADDITIONS TO THE BUDYKO-SELLERS EBM

Budyko-Sellers models traditionally only had a small number of parameters expressed in the model, and typically only conserved energy. The simple nature of the model type was a fertile bed for additional parameters and integration of new physical phenomena. This was often done with the aim of testing one new parameter on an EBM, in order to observe it in isolation rather than try and understand it in a more integrated, inter-connected model like a GCM.

For example, Rose and Marshall [52] [51] asserted that an important missing element in Budyko-Sellers models is that one of the largest components to meridional heat transport is missing: wind-driven ocean gyres. Gyres are large systems of rotating ocean currents, and on earth typically draw warm water from equatorial latitudes to cooler mid-latitudes, acting as a transporter of heat. By adding a conservation of momentum parameter, they captured this mechanism and observed that it allowed for a new stable solution (other than the ice free or ice covered solution), as a finite ice edge at the latitude corresponding to the centre of the gyre.

Dommenget and Flöter [13] demonstrated that with the addition of some parameters (mainly hydrological) and by resolving the model in two dimensions with distinct surface (with topography) and ocean

values, a solution with remarkable resemblance to empirical values could be produced. Zonal surface asymmetry between land and ocean, and also asymmetry between Northern and Southern hemispheres was explored by Hartmann and Short [22]. They found that the addition of zonal asymmetry increased the sensitivity to change in solar constant, and suggested that the Earth was more likely to go through abrupt state transitions (into snowball or ice free states) than EBMs had previously suggested. This result was in contradiction to the earlier result by Linzen and Farrell [36] that showed that extra parameterizations increased the stability, rather than reduced it.

Seasonal variations were added in multiple papers. Warren and Schneider [59] suggested that seasonal variation was a good test case for judging EBM accuracy, as it was a known forcing with previously measured responses. Graves et al. [19] noted that seasonal variation additions to EBMs only added a slight dependence to seasonal variation in the existing parameters, and that the the temperature sensitivity to changes in the solar constant was about the same as an EBM using annual mean values. North et al. [40] found that seasonal variations in snowline albedo, along with more realistic geography (their model was two dimensional, with discrete land and ocean areas) could cause the abrupt state change seen in EBMs, and this result was confirmed by Lin and North [35].

Parameters for greenhouse gases were added by Ikeda and Tajika (CO_2) [27], and Barker (CO_2, O_3) [4]. Greenhouse gases will not be dealt with in detail in this thesis (as mentioned in Section 1.2.3).

2.4 WATER IN STATES OTHER THAN ICE IN EBMS

Whilst all Budyko-Sellers models parameterise water in its solid state as ice, the standard model configuration does not explicitly deal with other states of water. Seller's original model includes cloudiness as some fixed adjustment parameter to zonal albedo, and suggested that while cloudiness would not be likely to change significantly to the planet as a whole, the meridional distribution would be significantly varied [53]. In fact, both water in vapour and liquid (cloud) states have a powerful effect on global energy balance. Importantly, the distribution and transport of water in various states would be significantly different during glaciation and ice-free phases of Earth's climate history [49], and Budyko-Sellers models do not address this.

Seller's choice of empirically defined cloud also falls short from a empirical viewpoint. Precipitable water vapour available for the formation of cloud is heavily determined by geographic features, and seasonal values differ markedly from inter-annual ones [23]. Two di-

mensional EBMs that take into account topography have confirmed this [13].

Explicit treatment of water in an EBM was first attempted by Roads and Vallis [50]. They calculated water parameters seperate to solving the EBM, so temperature feedbacks were not considered. Jentsch [29] was the first to add the surface humidity as a function of temperature to a two layered (atmosphere and ocean) EBM , thereby adding the whole hydrological cycle (in a simplified form) as a feedback in the same way that ice feedback was dealt with in EBMs previously. Humidity was tracked through all stages: evaporation at the surface layer, advection of vapour, condensation into clouds, and finally precipitation. Concentrating on just humidity alone as the new parameterized physical phenomenon allowed for both cloud feedbacks (positive and negative) and vapour feedback to be expressed. Jentsch found that the stability of the model increased overall, but that changes to surface humidity levels changed the position of "snowball" and ice-free solutions relative to the same changes in the solar constant [30]. This result was also found by Emanuel [14], who established that for any value of insolation at top-of-atmosphere, there are multiple stable solutions for a simple model, changing only the strength of cloud or vapour feedbacks. Jentsch's hydrological cycle was a fixed part of the model , and so his analysis was directed at varying the concentration of water vapour alone.

One thing that Jentsch's work also ignored is the ocean itself as an engine of heat exchange, rather than just a source of humidity. Ocean heat capacity is a perennial problem in the accuracy of EBM solutions. As EBMs balance only energy fluxes from surface to space, oceanic heat fluxes are not explicitly dealt with. One approach to accounting for the "lag" effect of the ocean's large heat capacity was developed by Bar-Eli and Field [3]. They added a time lag to feedbacks from cloud and ice/snow cover, stating that there was a "need to take into account in a manageable fashion time lags resulting from coupling of the very large heat capacity of the Earth with finite radiative-energy fluxes". This lag is also observed in much more complex ocean parameterizations, even in the absence of explicit time lag functionality [5]. Rose and Marshall [52] used a different approach to the ocean to solve this problem, adding a momentum conservation component, deciding that the most important aspect of the ocean's heat was it's ability to transport heat meridionally through wind-driven gyres. Their model added a new stable solution to their EBM on inclusion of this expansion of the model, at the centre of the mid-latitude gyres produced by the model. Hoffert et al [25] explictly added deep ocean

heat storage, and concluded that an EBM with a deep ocean layer for heat storage created a lag in heating effects.

Whether or not the addition of hydrological features increases or decreases the stability of the model is not clear. Jentsch's model is more stable than a standard Budyko-Sellers EBM, owing to IR damping and reduction of heat transport [30]. In an earlier result, this was partially predicted by Linzen and Farrell [36], who added several parameterizations (an approximation of a Hadley cell, atmospheric eddy transport term, and an ocean transport term) to an EBM and found that it decreased the overall sensitivity of the system. This view is not shared by Held and Soden [23], who stated that more feedbacks "potentiate" or strengthen sensitivity in the Earth system, particularly those feedbacks associated with water vapour. Cloud albedo and its interaction with surface snow/ice albedo is also still subject to large uncertainties in the literature [10]. Cloud is especially difficult because it represents both a positive and negative feedback to temperature, through absorption of longwave radiation and reflectance of shortwave radiation, respectively. At the poles this is compounded by the effect of negative cloud feedback in offsetting the albedo from ice cover below it, as the decreased air temperatures create lower levels of available water vapour [11].

Aerosols also potentially have an impact as they produce brighter clouds that are less efficient at releasing precipitation - the combination of the two effects reduces the amount of solar radiation that reaches the ground, producing a corresponding heating of the atmosphere and cooling of the surface [48]. In particular, carbonaceous aerosols like black carbon have only very recently had their impact on radiative forcing quantified [7].

2.5 POLAR AMPLIFICATION

Polar amplification is an effect where the poles display more sensitivity to increases in energy into the climate than lower latitudes, so that temperatures increase is greater in the polar region than the overall mean temperature increase for the whole Earth. The principal contributor is widely believed to be surface albedo feedback [2]. Alexeev and Jackson [2] found that atmospheric heat transport played no part in polar amplification. Graversen and Wang [18] produced results from a GCM with locked surface albedo (to remove the feedback effect) and still identified polar amplification, and suggested that greenhouse effects from a disproportionate increase in cloud and water vapour in the polar region versus the rest of the model may also play a part in the effect. Dommenget and Flöter [13] also found evidence that water

vapour was involved, through a combination of inhomogeneous distribution of water vapour in the Northern hemisphere and non-linear sensitivity of downward longwave radiation to water vapour density.

MODEL DEVELOPMENT

There is more to climate than temperature, but equally certainly temperature is a major part of what is meant by "climate", and greatly affects most of the other processes which come under the heading.

— Raymond Pierrehumbert

This chapter details the equations and their constituents that describe the EBM developed in this thesis. The structure of the description is from the top down - starting from the complete differential equations used to represent the model, each term in the differential equations is explored in turn, with physical explanations and justification for each term's values made following the definition of each term.

3.1 EBM EQUATIONS

Budyko and Seller's original models have only one driving differential equation for a unified surface/atmosphere [8] [53], and so are conceptually limited to considering a single temperature for each latitudinal zone. By separating this unified layer into two layers, different diffusion characteristics can be given for each layer, which is more realistic, and allows for more nuanced parameterizations to be used. Following Held and Suarez's two layer formulation [24], the general formulation of the differential equations can be written as:

$$C_a \frac{\partial T_a}{\partial t} = D_y \left(C_a K_a \frac{\partial T_a}{\partial \phi} \right) + LW_a + SW_a \tag{4}$$

$$C_s \frac{\partial T_s}{\partial t} = D_y \left(C_s K_s \frac{\partial T_s}{\partial \phi} \right) + LW_s + SW_s \tag{5}$$

Equation 4 represents the atmosphere layer, and Equation 5 represents the surface layer. "a" and "s" subscripts denote atmosphere and surface parameters, respectively. *LW* represents the collection of longwave parameters for a particular layer, and *SW* the shortwave parameters, which are derived in Section 3.2 and Section 3.3. "Longwave" and "shortwave" are used by convention to denote outgoing

terrestrial radiation and incoming solar radiation, respectively. Care should be taken in not conceptualizing these parameters in terms of defined ranges of wavelength (as both longwave and shortwave parameters encapsulate a large range of possible wavelengths), but instead thinking only of them in terms of transfers [6]. In this thesis, "shortwave" always denotes incoming solar radiation, and "longwave" always denotes radiation outgoing from a terrestrial layer.

The remaining term, which represents the meridional heat flux on the RHS of Equations 4 and 5, can be written as:

$$D_y\left(CK\frac{\partial T}{\partial \phi}\right) \tag{6}$$

where $\frac{\partial T}{\partial \phi}$ is the rate of change in temperature for the specific layer as a function of latitude, ϕ (in degrees). C is the heat capacity of a unit area atmospheric column (in units of $\text{Jm}^{-2}\text{°C}^{-1}$), and K is a diffusivity constant (in units of m^2s^{-1}). D_y is an operator representing the meridional divergence, which in terms of spherical geometry of the Earth can be represented as:

$$D_y = \frac{1}{2\pi a^2}\frac{d}{dx} \tag{7}$$

where a is the radius of the Earth, and the meridional term is resolved in a coordinate system using the sine of latitude $x = sin(\phi)$. Converting Equation 6 to this coordinate system, and combining Equations 6 and 7 yields:

$$D_y\left(CK\frac{\partial T}{\partial t}\right) = \frac{1}{2\pi a^2}\frac{d}{dx}\left[-2\pi(1-x^2)CK\frac{\partial T}{\partial x}\right] \tag{8}$$

It is important to note that the heat terms used by the EBM are simplified in such a way as to neglect latent heat and phase transitions: while these processes are clearly important to real heat content and transport in the climate, without explicitly conserving mass in the system this would be impossible to parameterize.
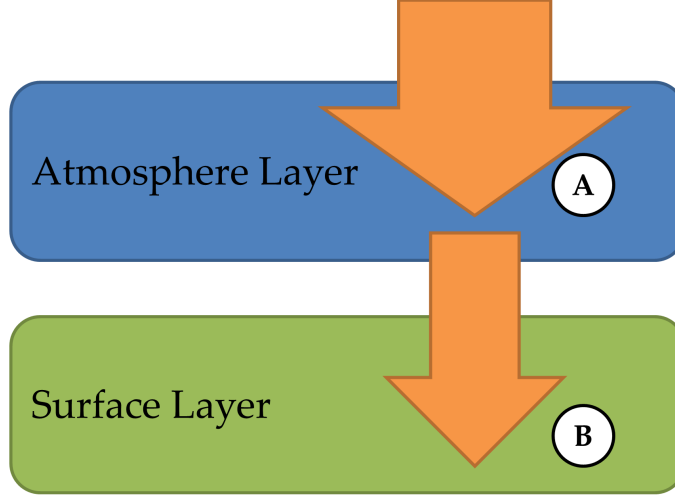
Figure 6: Shortwave radiative flux components.

Shortwave radiation in the model consists of all received radiation from the Sun. Figure 6 shows both elements of shortwave radiation, which are as follows:

- **A**: The portion of insolation that is absorbed by the atmosphere layer.

- **B**: The remaining portion of insolation that passes through the atmosphere, and is absorbed by the surface.

Component **A** can be written as:

$$SW_s = S(x)\frac{\tau(1-r_s)}{1-r_sr_a} \tag{9}$$

and component **B** can be written as:

$$SW_a = S(x)\left[1 - r_a - \frac{\tau(1 - r_a - \tau(\tau r_s + (1 - r_s)))}{1 - r_sr_a}\right] \tag{10}$$

where, as in Equations 4 and 5, the "s" subscript represents surface layer parameters, and "a" represents atmosphere layer parameters. Section 3.2.1 details each of the variables and components for

both parameters. r_a is the reflectivity of the atmosphere layer, r_s the reflectivity of the surface, and τ is the transmissivity. $S(x)$ is incoming solar radiation as a function of latitude. These variables are further defined in Section 3.2.1.

Both shortwave parameters used implement portions of the work of Jentsch [29], who introduced a comprehensive set of hydrological features into a Sellers-style EBM. Jentsch's work is especially useful in that the hydrological cycle is parameterized in such a way as to allow it to be separated from the basic heat diffusion parameters, as opposed to the traditional approach of a simple empirical adjustment of diffusivity. For example, Seller's model [53] does include the action of cloud, but only as an empirical adjustment to diffusivity, K, and so the individual action of cloud cannot be quantified. The motivation for using this approach is to be able to cleanly add or remove water features from the model, in order to examine their individual contributions to model behaviour.

3.2.1 *Shortwave Variables*

$S(x)$ in Equations 9 and 10 is an approximation to the observed annual mean distribution of solar radiation as a function of the sine of latitude: $x = sin(\phi)$ [41]. Having an insolation term in both layers is a departure from Held and Suarez's two layer model, which effectively treated the atmospheric layer as transparent to solar radiation. This was a reasonable assumption for a model with no parameterized water components, but for a model with hydrological features, the atmosphere will absorb both outgoing longwave radiation and at least some incoming shortwave radiation. $S(x)$ is determined by:

$$S(x) = \frac{S_0}{4}[1 + s_2 P_2(x)] \tag{11}$$

where $s_2 = -0.48$, and $P_2(x)$ is the second order Legendre polynomial. $S(x)$ is divided by four to represent the solar insolation for a latitude circle of a fixed latitudinal width (i.e. $\frac{1}{4}$ is the ratio of areas of a disk to sphere). The term in the square brackets in Equation 11 is developed from the first two even terms of a Fourier-Legendre series, with odd terms omitted, as $S(x)$ is an even function of x. This gives an insolation curve (Figure 7) within 2% accuracy to the mean annual insolation of Earth [41]. The value of s_2 has had several different interpretations since North introduced it, the value used for this model is from Rose and Marshall [52], which gives the most up-to-date approximation to the current observed annual mean distribution.
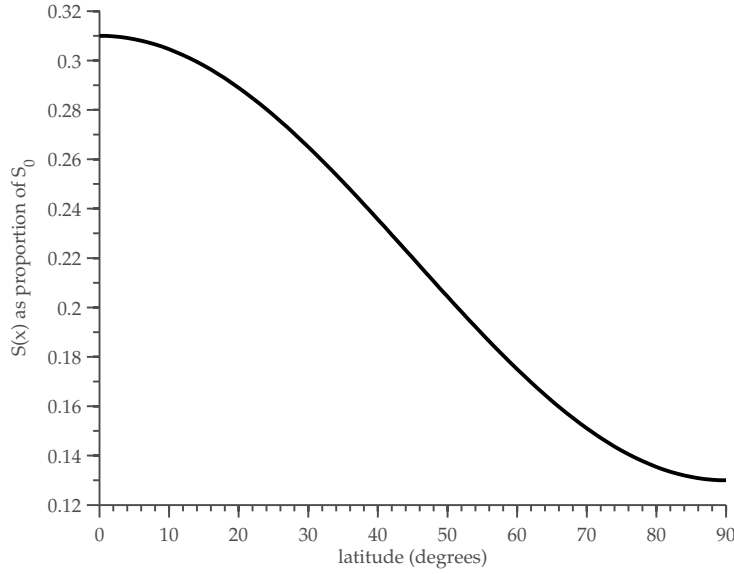
Figure 7: Curve of insolation given by S(x).

Reflectivity, absorptivity, and transmissivity (these terms are explained in Section 1.1.1) of the atmosphere layer are identified by r_a, κ_a, and τ, respectively. τ is defined as:

$$\tau = 1 - r_a - \kappa_a \tag{12}$$

Where the reflectivity r_a is given by:

$$r_a = cr_{cloudy} + (1 - c)r_{clear} \tag{13}$$

The transmissivity of the atmosphere is defined in Equation 12 as 100% effective, minus the amount of radiation reflected out of the layer (r_a), and the amount absorbed by it (κ_a). The reflectivity in Equation 13 is the total reflectivity of the atmosphere layer is a weighted sum of the reflectivity of cloudy sky (r_{cloudy}) and clear sky (r_{clear}), in proportion to cloud fraction, c.

The absorptivity κ_a is given by:

$$\kappa_a = c\kappa_{cloudy} + (1 - c)\kappa_{clear} \tag{14}$$

where again, the total absorptivity is the sum of the absorptivity of clear sky (κ_{clear}) and cloud-covered sky (κ_{cloudy}), weighted in proportion to cloud fraction.

κ_{cloudy} has been defined in [29] by:

$$\kappa_{cloudy} = \kappa_{clear} + 0.04 \tag{15}$$

Equation 15 represents that cloud is a slightly better absorber of shortwave radiation than clear sky. κ_{clear} is given as:

$$\kappa_{clear} = \kappa_0 + A_{water}(h) \tag{16}$$

where κ_0 represents absorptivity of completely dry air and $A_{water}(h)$ represents the absorption effect of water vapour, developed by Lacis and Hansen [32]:

$$A_{water}(h) = \frac{2.9h}{(1 + 141.5h)^{0.635} + 5.925h} \tag{17}$$

where h is the total column water vapour in centimetres, derived in section 3.2.1.2. Cloud fraction c is derived in section 3.2.1.3.

3.2.1.1 *Derivation of surface albedo, r_s*

The surface albedo, r_s, has two fixed values, for two modelled circumstances:

- **Ice covered albedo**: Albedo of a latitude band that is covered in ice. This is set for any latitude band with a surface temperature less than T_{crit}, which is defined as the temperature surface ice forms.

- **Non ice albedo**: Albedo of a latitude band that is ice free. Set for a latitude band with a surface temperature greater than $T_c rit$.

Some parts of the literature give more complicated functions for albedo, such as a gradiated transition between non-ice and ice to avoid a discontinuity. This approach was used by North [41] and Rose and Marshall [52], for example. This was specifically avoided in this model as the gradiated transition is justified by both papers as a way to account for shifts in cloudiness near the ice edge latitude, and since cloud is explicitly handled in the model, it is already accounted for.

3.2.1.2   *Derivation of total column water vapour, h*

Total column water vapour is the depth of water that would be found if an atmospheric column of some unit area had all it's water precipitated out as rain. Starting with an expression of the mass of water vapour in an atmospheric column with a cross-sectional area of A:

$$m_v = Am_w n_0 H \qquad (18)$$

where m_w is the mass of a water molecule, n_0 is the number density of water vapour molecules at the surface and H is the scale height. The scale height is the increase in altitude required to reduce the pressure by a factor of e. It is dependent on the molecular weight of the gas (or mix of gases), so different substances have different scale heights. H in this case is defined as the scale height of water vapour.

For the mass of liquid water in the column:

$$m_l = \rho_l Ah \qquad (19)$$

where ρ_l is the density of liquid water. Equating the mass of the water vapour column with the equivalent amount of liquid water in the same area column (i.e.equating 19) and (18):

$$\rho_l Ah = Am_w n_0 H \qquad (20)$$

Next the ideal gas law is invoked for water vapour at the surface, giving:

$$P_{v,0} = n_0 k T_0 \qquad (21)$$

where $p_{v,0}$ is the partial pressure of water vapour at surface, T_0 is temperature at surface, and k is the Boltzmann constant. Rearranging for n_0 gives:

$$n_0 = \frac{P_{v,0}}{kT_0} \qquad (22)$$

and then using it to substitute n_0 in Equation 20:

$$\rho_l Ah = \frac{AP_{v,0} m_w H}{kT_0} \qquad (23)$$

Cancelling A values in Equation 23, and finally rearranging for h gives the final form of h used in the model:

$$h = \frac{m_w P_{v,0} H}{kT_0 \rho_l} \qquad (24)$$

3.2.1.3 *Derivation of cloud fraction, c*

Starting with a surface partial pressure of water vapour for each latitude band as:

$$P_{v,0} = P_{H_2O} \times RH \tag{25}$$

Where RH is a fixed relative humidity, and P_{H_2O} is the saturation partial pressure of water vapour. P_{H_2O} is calculated using the Magnus approximation (Equation 26):

$$P_{H_2O} = C_1 exp(\frac{A_1 T}{B_1 + T}) \tag{26}$$

The Magnus approximation (also known as the August-Roche-Magnus formula) is an empirical approximation of the Clausius-Clapeyron relation, tuned for water vapour in typical atmospheric conditions, and is built such that temperature is the only independent variable. This allows for the calculation of saturation water vapour partial pressure in the atmosphere layer using only one prognostic variable, T, and an estimate of the mean relative humidity at the surface. The Magnus approximation is theoretically varied by the surface underneath the air column, and Alduchov and Eskridge [1] determined values for dry land, water, and ice. Observing the calculated partial pressure curves showed that surface choice made insignificant differences to their respective curves (Figure 8), and so dry land was chosen as the material for the model.

Then $P_{v,0}$ is recalculated for an atmosphere of a specific pressure altitude, which is converted to an altitude, z.

$$P_{v,atmo} = P_{v,0} e^{-z/H} \tag{27}$$

The dry air partial pressure is, invoking Dalton's law of partial pressures:

$$P_{dry,atmo} = P_{atmo} - P_{v,atmo} \tag{28}$$

Dalton's law is an empirical law which states that the total pressure exerted by the mixture of non-reactive gases is equal to the sum of the partial pressures of individual gases, and using this it can be said that that the partial pressure of dry air plus the partial pressure of water vapour in the atmosphere layer will approximately equal the total pressure of the atmosphere layer (a rearranged version of
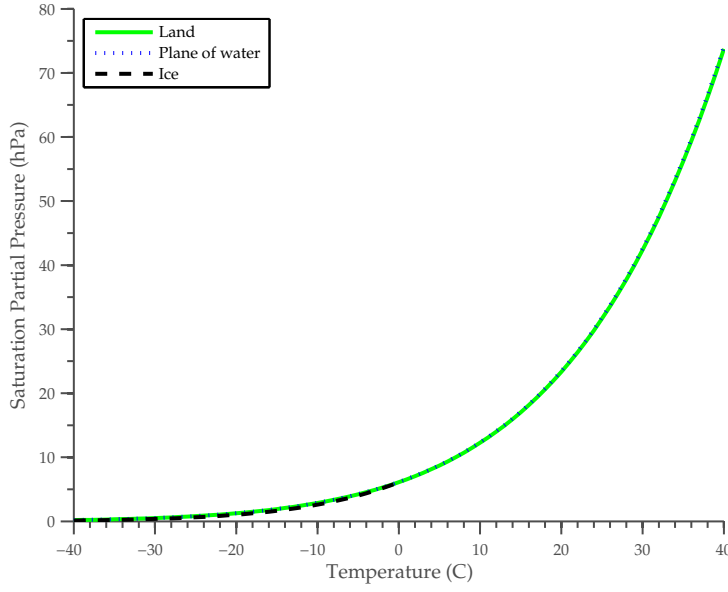
Figure 8: Magnus approximation for different surface materials, using values from Alduchov and Eskridge [1].

this relationship is shown in Equation 28). Then c, the cloud fraction is derived by calculating the relative humidity fraction given these partial pressures:

$$c = \frac{q}{q_*} \tag{29}$$

Where (from [29]):

$$q = \frac{P_v}{P_v + P_{dry}} \tag{30}$$

And from [38]:

$$q_* = \left(\frac{R_{dry}}{R_v}\right) \frac{P_{v,atmo}}{P_{dry,atmo}} \tag{31}$$

Equations 29, 30, and 31 are combined to give a final form of c for the atmosphere layer:

$$c = \frac{P_{dry,atmo} P_{v,atmo}}{\frac{R_{dry,atmo}}{R_{v,atmo}} P_{v,atmo} \left(P_{dry,atmo} + P_{v,atmo}\right)} \tag{32}$$
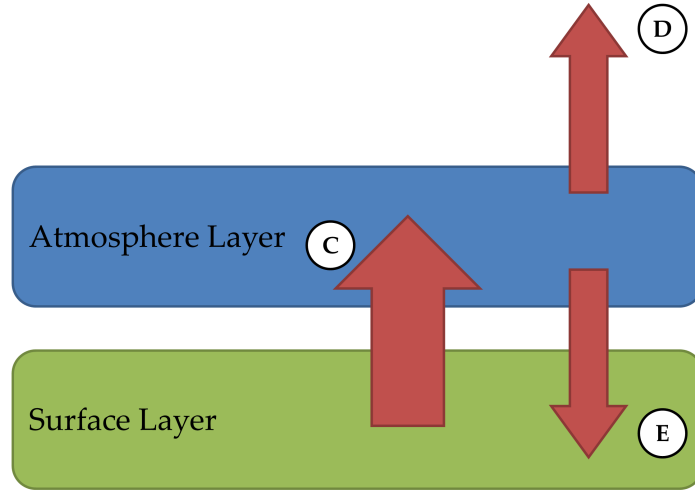
Figure 9: Longwave radiative flux components.

3.3 LONGWAVE PARAMETERS

Longwave radiation in the model consists of all emitted radiation from substances in both layers. Figure 9 shows elements of longwave radiation, which are as follows:

- **C**: Emitted longwave radiation from the surface layer. A proportion is absorbed by the atmosphere layer, which is dictated by γ, the deviation from perfect absorptivity or equivalently transmissivity of the atmosphere layer (Equation 39).

- **D** and **E**: Emitted radiation from the atmosphere layer. **D** is radiation that is lost to space, and **E** is longwave radiation that is re-absorbed by the surface layer. **D** and **E** are of equal magnitude.

The parameters in the model based on these radiative fluxes were defined using the Stefan Boltzmann law (Equation 1) and principles of emissivity and absorptivity (as described in Section 1.1.1). Starting with component **C** in Figure 9, the term for the amount of longwave radiation that is lost by the surface can be written as:

$$-e_s \sigma T_s^4 \tag{33}$$

where e_s is the emissivity of the surface layer, σ is the Stefan-Boltzmann constant, and T_s is the temperature of the surface latitude zone (as

temperature is function of latitude in the model). The proportion of this outgoing longwave radiation that is absorbed by the atmosphere layer is:

$$\gamma e_s \sigma T_s^4 \qquad (34)$$

where γ is a value that describes the absorptivity in the atmosphere due to H_2O, CO_2, and O_3, developed by Barker [4], which is derived in Section 3.3.1.

Components **D** and **E** are of equal magnitude, and can be written as:

$$e_a \sigma T_a^4 \qquad (35)$$

where e_a is the emissivity of the atmosphere layer, and T_a is the temperature of the atmosphere latitude zone. Since the atmosphere is losing twice this value (once up into space, and once down to the surface), the quantity of longwave radiation lost from the atmosphere layer is:

$$-2e_a \sigma T_a^4 \qquad (36)$$

Combining together Equations 34 and 36 gives the final atmosphere layer longwave radiation flux parameter, LW_a:

$$LW_a = \gamma e_s \sigma T_s^4 - 2e_a \sigma T_a^4 \qquad (37)$$

Combining Equations 35 and 33 gives the final surface layer longwave radiation flux parameter, LW_s:

$$LW_s = -e_s \sigma T_s^4 + e_a \sigma T_a^4 \qquad (38)$$

3.3.1 Derivation of Gamma

γ can be written as:

$$\gamma = 1 - \exp[0.082 - (2.38 P_{H_2O} H_{H_2O} R_H + 40.3 f_{CO_2})^{0.294}] \qquad (39)$$

Where P_{H_2O} is the saturation partial pressure of water vapour (calculated from Equation 26), H_{H_2O} is the scale height of water vapour

in kilometres, R_H is the relative humidity, and f_{CO_2} is the mixing ratio of carbon dioxide (3.5×10^{-4} corresponds to 350ppmv, for example). Equation 39 was derived from an approximation using an "equivalent widths" method, which gives an approximation of the integrated absorbance of the substance across the longwave wavelength band (Figure 2). The absorbance is then calculated as a function of concentration of CO_2 and H_2O, and the fitted curve gives the values to add to γ. The concentration of O_3 is fixed. The Barker γ was chosen as it allowed for a variance in H_2O, which means as moisture in the atmosphere is varied as a function of temperature (through processes used like the Magnus approximation in Equation 26) the absorbed longwave in the atmosphere can be adjusted accordingly.

3.4 FINAL EQUATIONS

Collating all the parameters explained in this chapter gives the final partial differential equations that the EBM uses:

$$
C_a \frac{\partial T_a}{\partial t} = \frac{1}{2\pi a^2} \frac{d}{dx} \left[-2\pi(1-x^2) C_a K_a \frac{\partial T_a}{\partial x} \right] + e_s \gamma \sigma T_s^4 - 2e_a \sigma T_a^4
$$
$$
+ S(x) \left[1 - r_a - \frac{\tau(1 - r_a - \tau(\tau r_s + (1 - r_s)))}{1 - r_s r_a} \right] \quad (40)
$$

$$
C_s \frac{\partial T_s}{\partial t} = \frac{1}{2\pi a^2} \frac{d}{dx} \left[-2\pi(1-x^2) C_s K_s \frac{\partial T_s}{\partial x} \right] - e_s \sigma T_s^4 + e_a \sigma T_a^4
$$
$$
+ S(x) \frac{\tau(1 - r_s)}{1 - r_s r_a} \quad (41)
$$

Equations 40 and 41 are classed as parabolic partial differential equations (PDEs). The method used to solve these equations is discussed in Section 3.6.

3.5 1, 2, AND 3 PHASE MODEL RUN VARIANTS

In order to examine the behaviour of the model with different phases of water included, three variants of the model were created:

- "1 Phase" - for a single phase of water, i.e. only surface ice, with no cloud or water vapour in the atmosphere.

- "2 Phase" - for two phases of water, surface ice and water vapour in the atmosphere, with no cloud.

- "3 Phase" - full model with all three phases of water represented, surface ice, water vapour, and cloud.

These three model regimes can also be thought of as models containing one, two, and three feedbacks, as each phase of water contains it's own climatic feedback process. The designations "1 Phase", "2 Phase", and "3 Phase" will be used as shorthand to designate these three different models for the rest of the thesis. Table 1 lists the changes to the model required to run each variant.

MODEL VARIANT	VARIABLE CHANGED
1 Phase	Relative humidity: $RH = 0$ for all latitudes, for all time steps
2 Phase	Cloud fraction: $c = 0$ for all latitudes, for all time steps
3 Phase	Complete model

Table 1: EBM variants.

3.6 NUMERICAL SOLUTIONS

The EBM was solved using a forward time central space (FTCS) finite difference method. This method was chosen over another method called the Crank-Nicolson method, as the Crank-Nicolson method gave solutions with small persistent oscillations in the equilibrium position of the ice edge, which would not dissipate with time as Crank-Nicolson is strictly non-dissipative [16]. Non-dissipative means that oscillations in the solution will never decrease with increasing time steps of the solution, and adding damping parameters to the final equations to solve this was thought to add inaccuracy to the solution. It would be theoretically possible to create damping parameters that

did not make the solution less accurate, but this fell outside the scope of the thesis (but could be done in future studies of the model).

The FTCS scheme can be proven to be accurate using the Lax-Richtmyer equivalence theorem, which is a theorem that allows for numerical approximations like FTCS to be considered convergent on the real solution of the PDEs used [55]. It states:

> *A consistent finite difference scheme for a partial differential equation for which the initial value problem is well-posed is convergent if and only if it is stable.*

where the technical terms in the theorem are:

- **Convergent:** A scheme is said to be *convergent* if its solutions approximate the solution of the PDE and that approximation improves as the grid spacings h and k tend to zero.

- **Consistent:** A scheme is said to be *consistent* if the approximate solution is pointwise convergent on the PDE at each grid point.

- **Well Posed:** A set of initial conditions is said to be well-posed if it produces a solution and that solution is unique and the solution is consistent for a small variation in those initial conditions.

Since the FTCS is *consistent* and the EBM equations are *well posed* (i.e. they do not wildly diverge for similar initial conditions except for near state transitions), and the FTCS scheme is stable for the EBM equations, the FTCS method is therefore convergent on real solutions for the EBM equations.

3.7 BASIC MODEL BEHAVIOUR
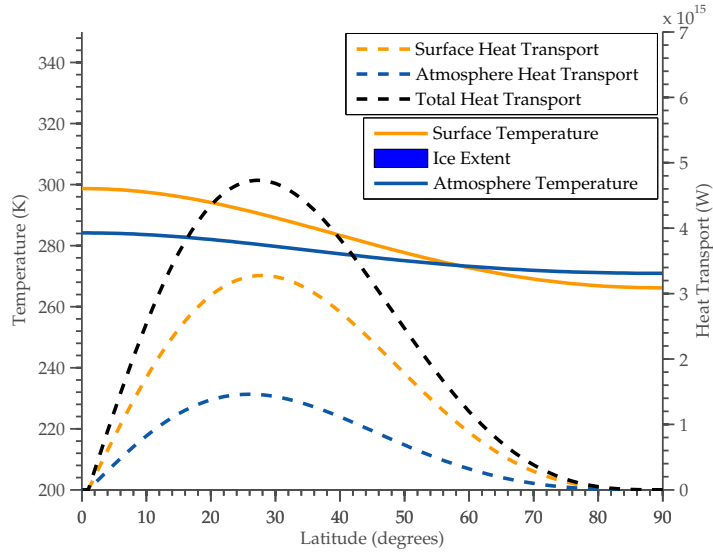
(a) 1 phase run.
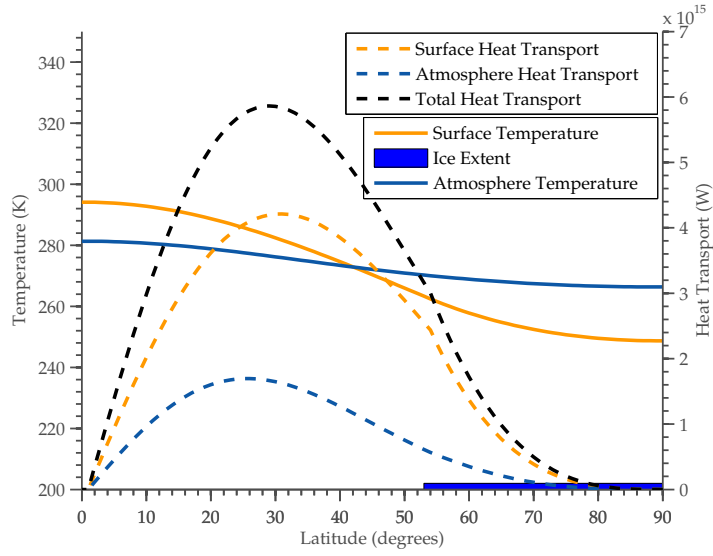
(b) 3 phase run.

Figure 10: 1 and 3 phase model runs using $S_0 = 1366\,\mathrm{Wm}^{-2}$.

Using the FTCS method detailed in Section 3.6, the model was run for $S_0 = 1366\,\mathrm{Wm^{-2}}$ for a 1 phase model (results in Figure 10a), and for a 3 phase model (results in Figure 10b). The equilibrium ice edge position is plotted as the extent from the right hand side of the axis. The largest difference between the two runs is that for $S_0 = 1366\,\mathrm{Wm^{-2}}$, the 1 phase model is in the ice free state (no ice is visible in plot) while the 3 phase model is in the finite ice edge state. Equatorial temperatures are similar between the two models, but the 1 phase model has a significantly warmer polar region (266.2 K at 90 degrees latitude, versus 248.7 K for the 3 phase model). This lessens the temperature gradient between equator and pole at the surface, and therefore reduces meridional surface heat transport (maximizing at $3.27 \times 10^{15}\,\mathrm{W}$, versus $4.21 \times 10^{15}\,\mathrm{W}$ for the 3 phase model), as temperature gradient is an integral part of calculating heat transport - see Equation 8). An inflection point in the surface heat transport can also be observed at 54 degrees in the 3 phase model run, which is approximately at the ice edge - this shows that the ice has a significant effect on heat transport. The inflection point was not observed in the 1 phase run, due to a lack of surface ice. The atmospheric heat transport were was only slightly lower in the 1 phase model (maximizing at $1.46 \times 10^{15}\,\mathrm{W}$ for the 1 phase model, versus $1.70 \times 10^{15}\,\mathrm{W}$ for the 3 phase model).
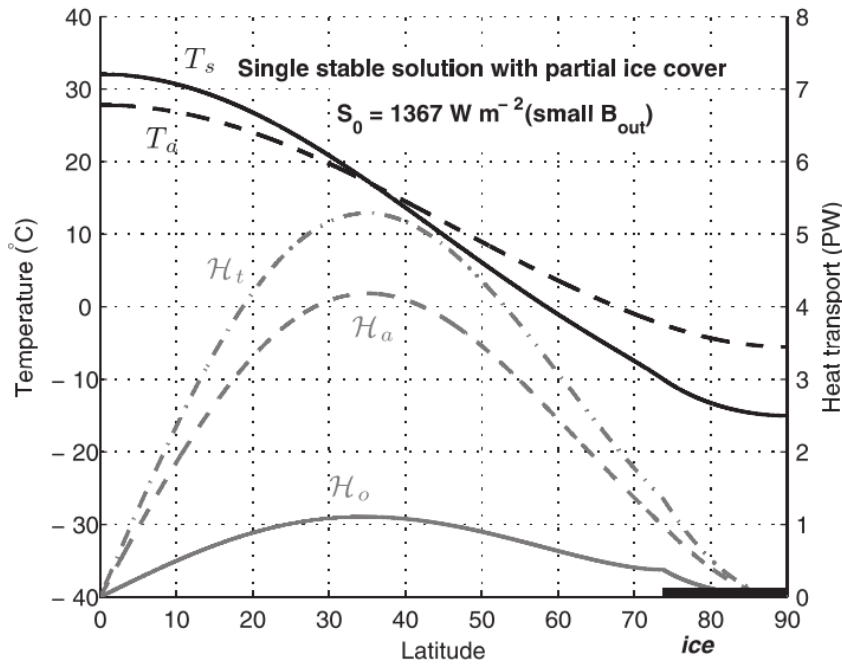
Figure 11: Rose and Marshall two layer model run. T_s and T_a are the surface and atmosphere layer temperatures, respectively. $\mathcal{H}_a$ is the atmospheric heat transport, $\mathcal{H}_o$ is the ocean heat transport, which is analogous to surface layer transport in the EBM used in this thesis.

An example two layer (atmosphere and ocean) EBM run from Rose and Marshall [52] is shown in Figure 11. Comparing the Rose and Marshall result to the EBM, shape and structure of temperatures and heat transports as functions of latitude were comparable Rose and Marshall's, but the magnitudes of heat transport are smaller, and the surface layer has a larger peak heat transport than the atmosphere layer, which is the reverse of the result from Rose and Marshall, and is not realistic. This is probably due to the atmosphere having a smaller temperature gradient between equatorial and polar latitudes than Rose and Marshall's model, which would have the effect of restricting heat transport. The small temperature gradient may have been caused by the atmospheric diffusivity K_a constant being too large, but this was tested by reducing it for subsequent runs and no significant temperature gradient increase was found, until eventually K_a became low enough that the model simply failed to converge to a solution.

3.8 TABLE OF VARIABLES & CONSTANTS

This section contains all values used for running the EBM, and their sources. Some experiments changed one or more of these variables in order to explore phenomena, and these changes are listed with each experiment.

VARIABLE	VALUE	SOURCE
A_1	17.625	[1]
B_1	243.04	[1]
C_1	6.1094	[1]

Table 2: Magnus Approximation constants.

VARIABLE	SYMBOL	VALUE	SOURCE
O_3 emissivity deviation	..	0.082	[4]
CO_2 emissivity deviation	f_{CO_2}	3.5×10^{-4}	[4]

Table 3: Values used in Barker's γ parameter.

VARIABLE	SYMBOL	VALUE	SOURCE
Relative Humidity	R_H	80%	..
Second Legendre polynomial fitting variable	s_2	-0.48	[52]
Absorptivity of dry air	κ_0	0.05	[29]
Reflexivity of cloudy sky	r_{cloudy}	0.2962	[58]
Reflexivity of clear sky	r_{clear}	0.1	[29]
Scale Height of water vapour	H_{H_2O}	2km	[4]
Scale height of atmosphere	H	8.5km	[39]
Density of liquid water	ρ_l	$1000\,\mathrm{kgm^{-3}}$	..
Initial atmosphere temperature	$T_{a,i}$	255K	[52]
Initial surface temperature (non-ice)	$T_{s,i}$	290K	[52]
Initial surface temperature (ice)	$T_{i,i}$	255K	[52]
Critical temperature of melting ice zone	T_{crit}	263K	[41]
Heat capacity of atmosphere column	C_a	$10^7\,\mathrm{Jm^{-2}}$	[43]
Heat capacity of surface/ocean column	C_s	$10^7\,\mathrm{Jm^{-2}}$	[52]
Diffusivity of atmosphere layer	K_a	$2.2 \times 10^6\,\mathrm{m^2s^{-1}}$	[52]
Diffusivity of surface layer	K_s	$5.2 \times 10^5\,\mathrm{m^2s^{-1}}$	[52]
Radius of Earth	a	$6371000\,\mathrm{m}$	[39]
Dry air specific gas constant	R_d	$287.058\,\mathrm{Jkg^{-1}K^{-1}}$	..
Water vapour specific gas constant	R_v	$461.5\,\mathrm{Jkg^{-1}K^{-1}}$	..
Surface pressure	$P_{surface}$	$1.014 \times 10^5\,\mathrm{Pa}$	[39]
Default atmosphere pressure	P_{atmo}	$0.5 \times 10^5\,\mathrm{Pa}$	[24]
Surface albedo (ice covered)	r_s	0.6	[41]
Surface albedo (ice free)	r_s	0.3	[41]

Table 4: Variables used in EBM.

4

SENSITIVITY

Sensitivity studies for energy balance models are collections of model runs that test the equilibrium response and characteristics of the model. They test the internal stability of the model by varying some prognostic variable for each run in the collection, while leaving the others static. They are often used to determine the strength and sign of various feedback mechanisms in the climatic system [30]. Testing the transient nature of models is outside the scope of sensitivity tests as they only view the model from its completed equilibrium position, and so transient effects will be dealt with separately in the stability chapter of the thesis (Chapter 5).

Equilibrium is not trivial to define for EBMs with non-linear feedback effects, as models can reach a quasi-stable state in one solution space before reaching some threshold and consequently shifting to a second equilibrium in another state. Jentsch defined equilibrium as having reached some point where the time rate of change of the global temperature was less than a small amount (order of 10^{-11} K) [29]. This however ignores boundary cases where the model may just have enough/too little heat to move to another solution state. To address this, the model has additional logic, so that the global energy balance must maintain its minimal value of energy balance change for a set number of time steps. For each model run, the model was resolved to a stable equilibrium state.

Table 5 lists all variables used to test the sensitivity of the model. Excluded from the list is the sensitivity of the model to different water phase feedbacks, which rather than varying some prognostic variable,

PROGNOSTIC VARIABLE	SYMBOL	RANGE OF VALUES
Atmosphere Layer Pressure	P_{atmo}	100 hPa to 700 hPa
Surface Albedo	r_s	ice albedo from 0.4 to 0.8,
		non-ice albedo from 0.1 to 0.5
Relative Humidity	RH	60% to 80%

Table 5: Prognostic variables used in sensitivity studies.

consist of switching these feedbacks on and off. Sensitivity to these components is detailed in Section 4.1.

Atmospheric layer pressure was chosen as it defines the height of the atmosphere layer, and as the water vapour pressure is defined by this height (Equation 27 in Section 3.2.1.3), this affects the amount of water vapour and cloud available. Thus, varying this parameter effectively varies the strength of cloud and water vapour feedbacks. Surface albedo was chosen because it is a good proxy for the strength of the surface ice feedback. Relative humidity was chosen as it is a good metric for water vapour feedback, as it affects the amount of water vapour on the surface (Equation 25 in Section 3.2.1.3), which in turn affects the amount of water vapour in the atmosphere.

4.1   SENSITIVITY TO WATER PHASE FEEDBACKS

4.1.1   *Sensitivity Study Method*

This section details general sensitivity results for the model by adding or removing water in each of the three phases it is found in Earth's climate. Sensitivity to changes in the solar constant, S_0, were used as the control variable. S_0 values were tuned by multiplying the raw S_0 with a tuning constant such that for $1366 \, \mathrm{Wm^{-2}}$, an ice edge as close to 72 degrees latitude as possible was formed for the 3 phase model. This tuning constant was then applied to all runs of the model shown in the results. It was not possible to give exactly 72 degrees in some cases, due to the existence of varying strengths of small ice edge instabilities (SICIs), described in Section 2.2.1, so in that case the highest stable finite ice edge is assigned to $1366 \, \mathrm{Wm^{-2}}$.

Definitions of the model variant names "1 phase", "2 phase", and "3 phase" are given in Section 3.5.

4.1.2   *Results*

Figure 12 shows model sensitivity to either 1, 2, or 3 phases of water feedback (described in Section 4.1). The figure shows three solution states to the model depending on the value of S_0:

- **Snowball Earth State**: For low values of S_0, the equilibrium ice edge stays at 0 degrees latitude, representing a "snowball" earth state - total ice cover of Earth.
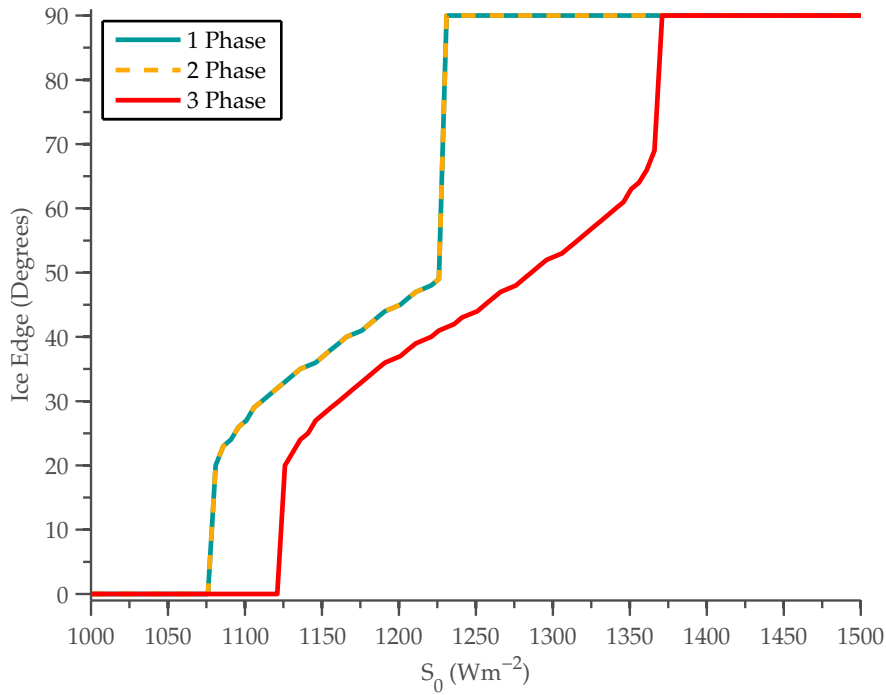
Figure 12: Model sensitivity to different 1,2, or all 3 phases of water feedback.

- **Finite Ice Edge State**: For medium values of S_0, equilibrium ice edge is between 0 and 90 degrees latitude, representing a finite ice edge state, the state Earth is currently in.

- **Ice Free State**: For high values of S_0, equilibrium ice edge stays at 90 degrees latitude, representing an ice free state - all polar ice on Earth has melted.

These terms will be used to describe the three states of the EBM for the remainder of the thesis.

Examination of Figure 12 shows that 1 and 2 phase models have very similar curves, which was found to be caused by a systematic underestimation of water vapour in the surface layer, which is detailed in Section 4.5. Due to this lack of meaningful difference with the 1 phase model, after initial analyses the 2 phase model was removed from figures in the rest of the studies in this chapter.

The 3 phase model displayed significantly weaker small ice edge instability effects (see Section 2.2.1 for details of the SICI phenomenon) than the other two models. Lee and North [33] had shown that the SICI effect is reduced in the presence of small fluctuations in model forcings [33], and this may be the case here - the cloud feedback may

be causing small variations in radiation flux, enough to recreate this effect. The reason cloud feedback may be involved is that since cloud fraction is affected by the temperature of the surface layer (as this affects the amount of water vapour available for cloud production, from the Clausius-Clapeyron relation and derivations in Section 3.2.1.3), the combination of heat transport and changing radiation flux to the surface from more/less cloud, these small variations can act similar to a noisy forcing term as used by Lee and North to reduce the SICI effect.

The 1 and 2 phase models moved away from snowball Earth states for S_0 values of approximately $100 \, \mathrm{Wm}^{-2}$ less than the 3 phase model. This is due to cloud absorbing more heat into the atmosphere layer in the 3 phase model, and also reflecting some radiation back into space, adding an extra negative radiative feedback that the cloudless model does not have, so that more radiation overall is required to get the equator latitude surface above T_{crit} so that the ice can begin to melt.
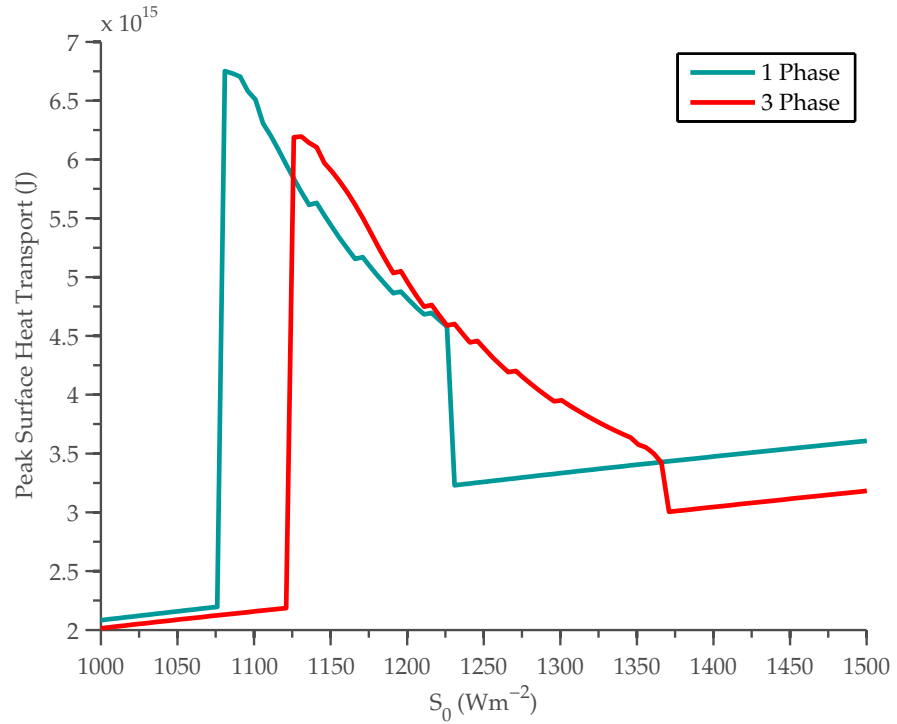

Figure 13: Peak surface layer heat transport as a function of insolation.

Figure 13 shows the peak heat transports for 1 and 3 phase models for the surface layer of the model, as a function of S_0. Figure 14 shows the same value for the atmosphere layer. These values were determined by calculating the heat transport function (Equation 8 in Section 3.1) for all latitudes with the temperatures of those latitudes
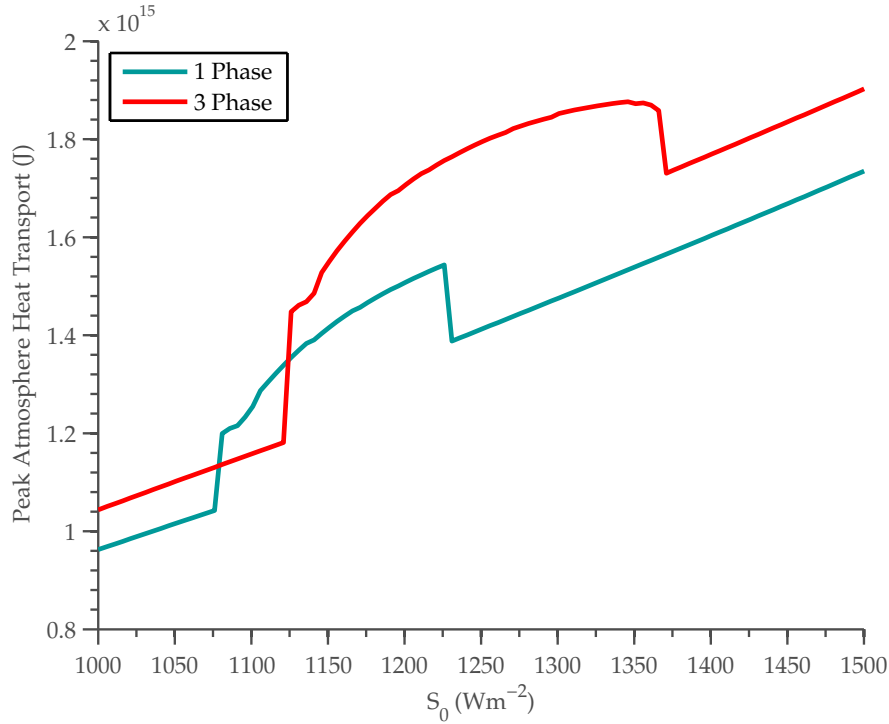
Figure 14: Peak atmosphere layer heat transport as a function of insolation.

at the equilibrium step (i.e. the last time step), and then determining the maximum of the heat transport function. The heat functions were calculated using the temperatures of each layer in question separately.

Surface heat transport peaks higher in the 1 phase model than the 3 phase model, but atmosphere layer heat transport peaks higher in 3 phase than 1 phase. Heat transport in the model is determined by the magnitude of temperature gradient between any two latitude zones, so this result means that the temperature gradient has the potential to be greater at the surface when water vapour and cloud are not present.

Both Figures 13 and 14 show that for snowball and ice-free solution states, peak heat transport is a linear function of S_0, which is expected for a 1 phase model, but was an unexpected result for the 3 phase model. The reason for this is for a 1 phase model, the only source of non-linearity is the surface ice feedback, which has a fixed effect when the ice edge is locked at 0 or 90 degrees - only when the ice edge moves (i.e. when the model is in the finite ice edge state) will the feedback change. For the 3 phase model, cloud and water vapour feedbacks are acting in all three states of the model. This means that peak heat transport would be expected to show more complex effects in the snowball and ice free states. One possible explanation is that

peak heat transport is occurring at the poles, where low cloud fractions and water vapour densities exist, meaning that cloud and water vapour feedback there can have little or no direct effect on the temperature gradient.

In Figure 13, the peak heat transport for both models occurs just after the transition into a finite ice edge state (i.e. when the ice edge is just retreating from the equator). This is an effect of the heat transport parameterisation in the model, which is calculated by the gradient of temperatures between any two points (Equation 8 in Section 3.1). The steepest gradient would then be at the ice edge discontinuity.

The reason for this is that coming out of a snowball state, the first latitude zone to become ice free will be the zone closest to the equator. This means that at this point there is an ice free latitude receiving the largest amount of insolation in the model (due to the geometric distribution of insolation seen in Figure 7 in Section 3.2.1) and it is adjacent to a latitude zone that is still ice covered, and so has most of its insolation reflecting away. This leads to the greatest possible temperature difference between the two zones, maximizing the temperature gradient, and therefore giving the greatest possible heat transport.

Each zone after the equatorial zone that is freed from ice as the model receives progressively larger values of S_0 will provide progressively smaller temperature differentials with the next ice zone adjacent, and this can be observed in Figure 13 as the curve of finite ice edge state peak heat transport approximately follows the insolation curve seen in Figure 7.
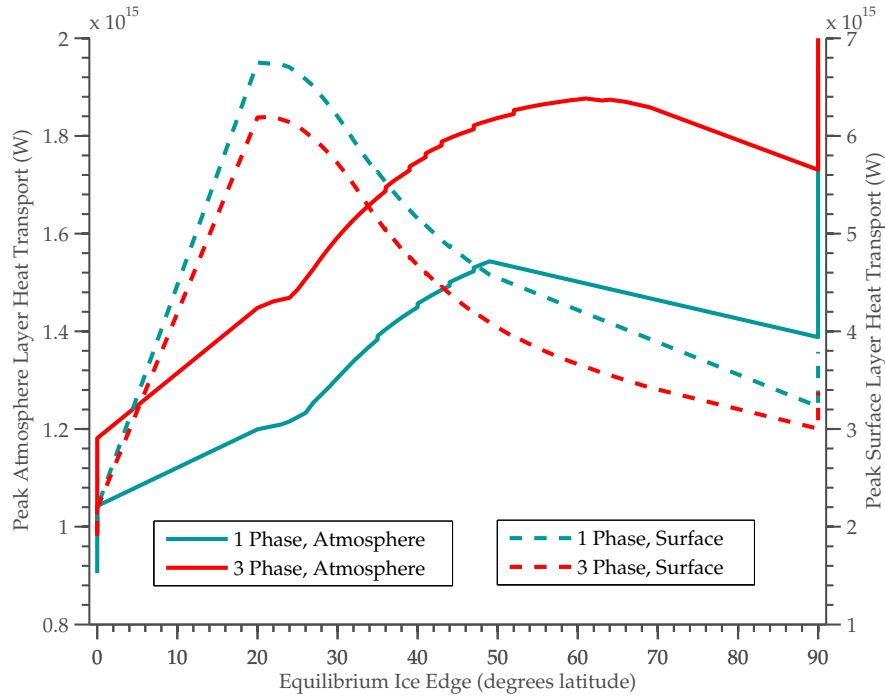
Figure 15: Peak heat transports as function of equilibrium ice edge.

Figure 15 shows peak heat transport as a function of equilibrium ice edge. This shows that overall, the 3 phase model's atmospheric heat transport has a greater proportion of total heat transport compared to the surface, compared to the 1 phase model. This can also be shown by examining the ratio of the means of heat transport for both 1 and 3 phase models:

$$\text{ratio} = \frac{\text{mean(surface heat transport)}}{\text{mean(atmosphere heat transport)}} \tag{42}$$

The ratio value for the 1 phase was determined to be 2.4953, and for the 3 phase model was determined to be 2.0626. This shows that the 3 phase model has a greater proportion of heat transport in the atmosphere layer compared to the surface layer. This effect is due to cloud (which is only in the 3 phase model) being a greater absorber of radiation than clear sky, and also due to less shortwave radiation reaching the ground due to reflection by cloud. For both models, surface heat transport is still much greater than atmospheric heat transport, a phenomenon also shown in all model variant's standard behaviour, and this is problematic as it is not a result seen in other similar models in the literature (Section 3.7).
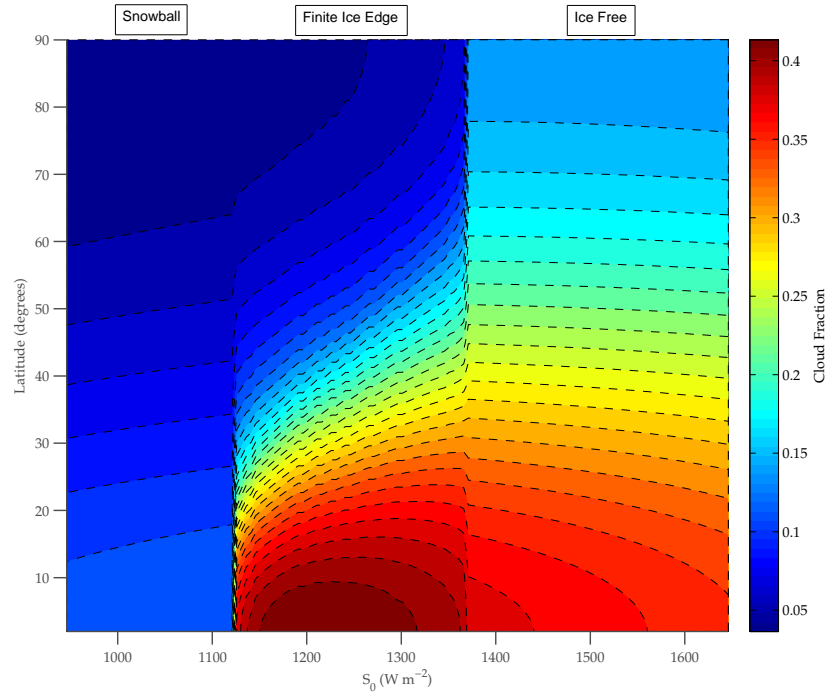
Figure 16: Cloud fraction for 3 Phase model for varying S_0. States of the model that ranges of S_0 lie in are annotated above the graph.

Figure 16 shows the fraction and latitudinal distribution of cloud in the model, for the 3 phase variant. The three solution spaces (snowball, finite ice edge, and ice-free) can be seen as three distinct patterns as S_0 is increased. As cloud fraction is derived from moisture parameters in the surface layer, the underlying reason for a lack of cloud in the snowball solution is because the surface is too cold to produce any significant cloud as the saturation water pressure at the surface is low, which restricts the amount of water vapour available for cloud production.

In the ice free solution space, the cloud fraction is observed to slowly decrease as S_0 is increased. This is not realistic as increasing atmospheric and surface temperatures should increase the saturation water pressure of the atmosphere to hold moisture. The Magnus approximation (Equation 26) used by the model to calculate water vapour partial pressure always increases with temperature, so intuitively, the model should reflect this. The low cloud fraction therefore implies that the surface layer is increasing in temperature slower than the atmosphere layer. This in turn means as the atmosphere takes a greater proportion of insolation than the surface, there is a corresponding decrease in the amount of cloud.
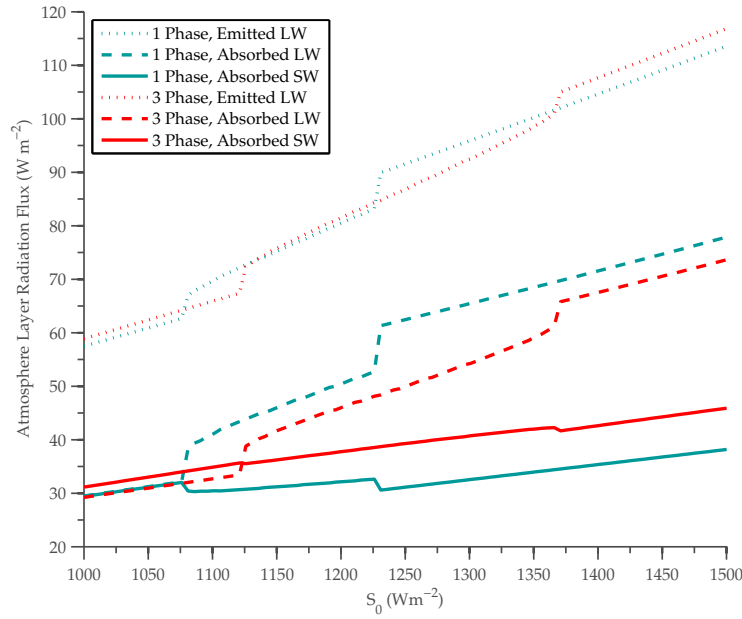
Figure 17: Components of atmosphere layer radiation flux.

Figures 17 and 18 show components of radiation flux (both absorbed and emitted) for 1 and 3 phase models. Figure 17 shows emitted/absorbed components from the atmosphere layer, and Figure 18 from the surface layer. Values are derived from components of the model detailed in Chapter 3, with absorbed shortwave values coming from equations in Section 3.2, and emitted/absorbed longwave values from equations in Section 3.3. To a good approximation, the sum of incoming components and the sum of outgoing components of flux appear to add to the same value - a good indicator that the model equations are balancing radiative components.

The step-like structure of the plotted curves is due to transitions between states of the model. Surface shortwave absorbance is the largest component of available heat in the model, other than meridionally transported heat, and so it causes all curves to have step changes when ice is removed, due to the discontinuous increase in available energy. This also accounts for the non-flat curve of radiation as a function of S_0 for the finite ice state (the center step), as the mean albedo of the surface is changing. Overall, more energy is available in the 1 phase model because less radiation from the atmosphere is being reflected away by cloud, allowing a greater amount to reach the surface, and this has the effect of reducing the extent of finite state solution space for the S_0 sensitivity study - the 1 phase model reaches a critical total energy required for transition to the ice-free state quicker than the 3 phase model does. The gradients of radiation increase as a
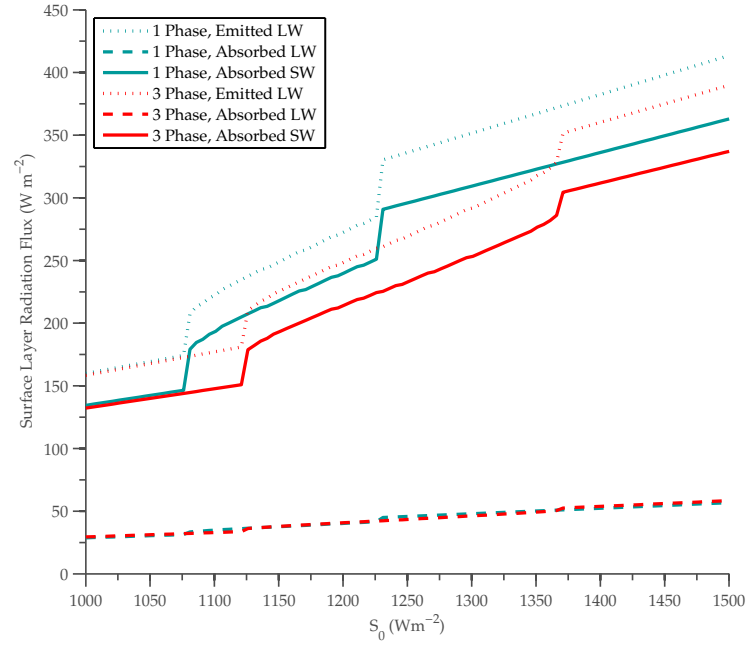
Figure 18: Components of surface layer radiation flux.

function of S_0 is effectively the same between 1 and 3 phase models, so this result does not imply that the 3 phase model is more stable, just that it is receiving less radiation for any given value of S_0 than the 1 phase model.

4.1.3 *Polar Amplification*

The water phase sensitivity studies were checked for evidence of polar amplification, an effect explained in Section 2.5. The sensitivity to changes in S_0 for both 1 and 3 phase models was observed by recording the gradient of mean temperature change per unit change of S_0 in the sensitivity test for two zones:

- **Polar Zone**: Latitudes from 70 to 90 degrees.

- **Non-Polar Zone**: Latitudes from 0 to 70 degrees.

The latitude ranges used are rough approximations of polar and non-polar latitudinal zones (the exactness of latitudes chosen is less of an important consideration for a one-dimensional EBM than if the model was two dimensional and had distinct land masses to give more complicated polar phenomena). If polar amplification is occurring then the polar zone should have a larger gradient than the non-polar zone.
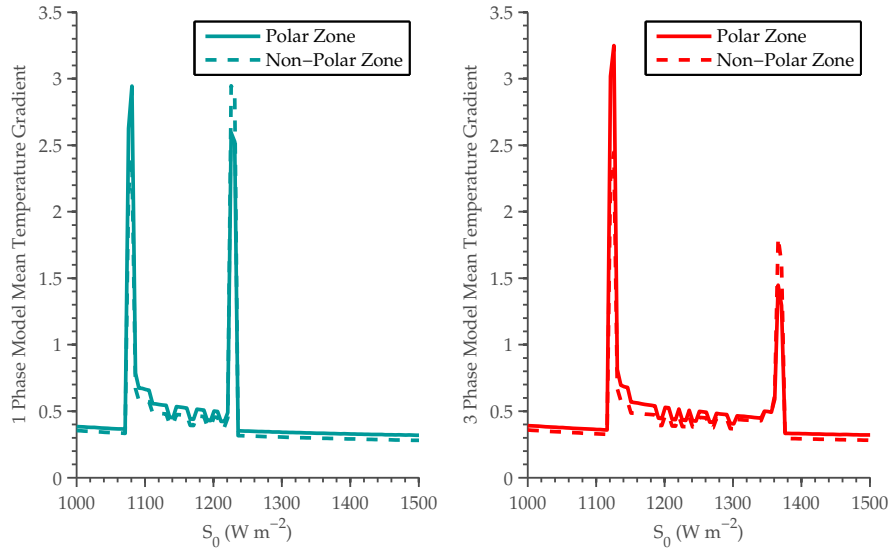
4.1.3.1 *Results*

Figure 19: Evidence of polar amplification effects in EBM. Left: 1 phase model run, right: 3 phase model run.

Figure 19 shows that for both 1 and 3 phase models, the polar zone mean temperature was more sensitive (the rate of change was greater) to increasing S_0 than the non-polar zone for most of the sensitivity run. Significant spikes in the gradients occurred where the model changed states, and here the amplification result is less clear.

The difference of gradients between polar and non-polar zones was calculated as:

$$\text{gradient difference} = (\text{polar gradient}) - (\text{nonpolar gradient}) \quad (43)$$

for all values of S_0. A positive value would mean that the polar gradient was greater than the non-polar gradient for that value of S_0. The results (Figure 20) show that the gradient difference is always positive, and so polar amplification is always occuring, even in the less clear areas near the state transitions. The 3 phase model showed a stronger amplification effect for the snowball state (low S_0) and most of the finite ice edge state (mid S_0). The difference was negligible for the ice-free state. This is expected as the impact on polar amplification by ice feedback has been effectively removed by loss of ice in the ice free state. The strengthening of the polar amplification effect with the addition of cloud (at least for most of the sensitivity run) agrees with the results of Graversen and Wang [18], and suggests that that changes
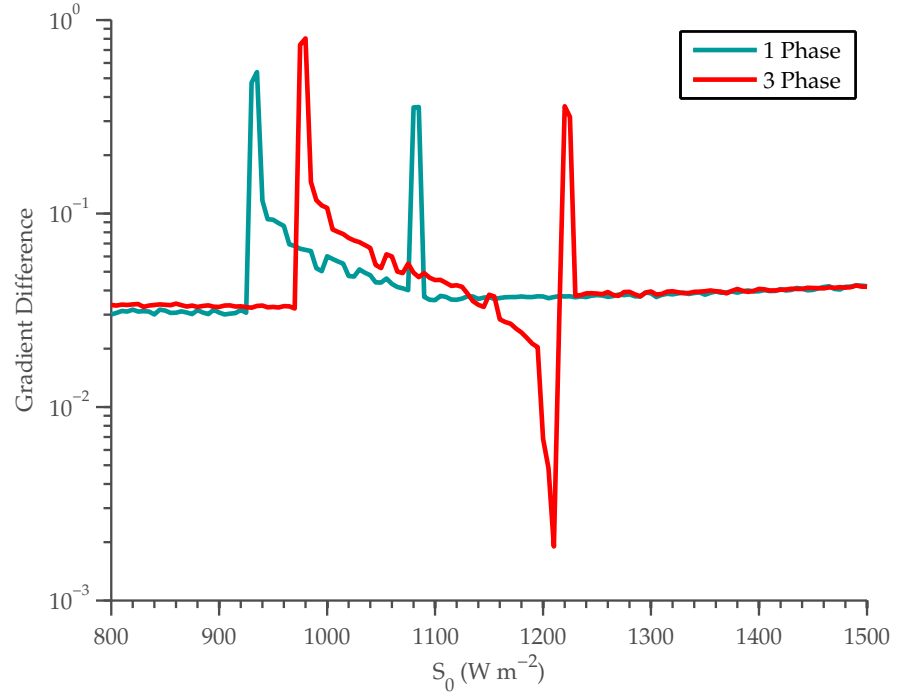
Figure 20: Gradient difference for polar and non-polar zones, calculated with Equation 43.

in radiative balance due to the addition of cloud may increase the amplification effect.

4.2 ATMOSPHERE LAYER PRESSURE SENSITIVITY

The prognostic variable that was varied in this study was P_{atmo}, the pressure level of the atmosphere layer. This affects the quantity of water vapour in the atmosphere layer (Equation 27 in Section 3.2.1.3), and so is a good way to adjust both cloud and water vapour levels. Held and Suarez [24] defined the atmosphere layer in their model being approximately at the boundary layer at a pressure level of $0.5 \times 10^5 Pa$, and so this can be considered the standard value (as used in other runs of the model in this and other chapters, see Table 4).
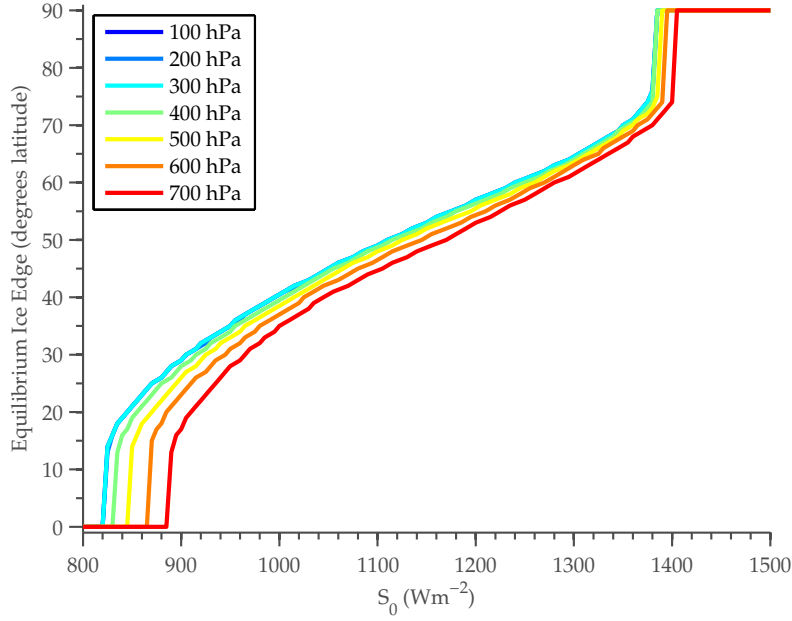
4.2.1   *Results*

Figure 21: Model sensitivity to atmosphere layer pressure level, P_{atmo}

Figure 21 shows the model's sensitivity to changes in the atmosphere layer pressure level, P_{atmo}. The transition from snowball to finite ice edge is seen to occur for higher and higher values of S_0 as pressure is increased. This is consistent with the results from Section 4.1.2, showing that an increase in cloud lowers the amount of radiation reaching the surface (from reflection of shortwave) and also shifts some heating to the atmospheric layer from absorbance of shortwave. The shape of the curve stays relatively similar for all pressure levels.

4.3   ALBEDO SENSITIVITY

The prognostic variable that was the albedo of the surface. Both ice and non-ice albedos were varied.
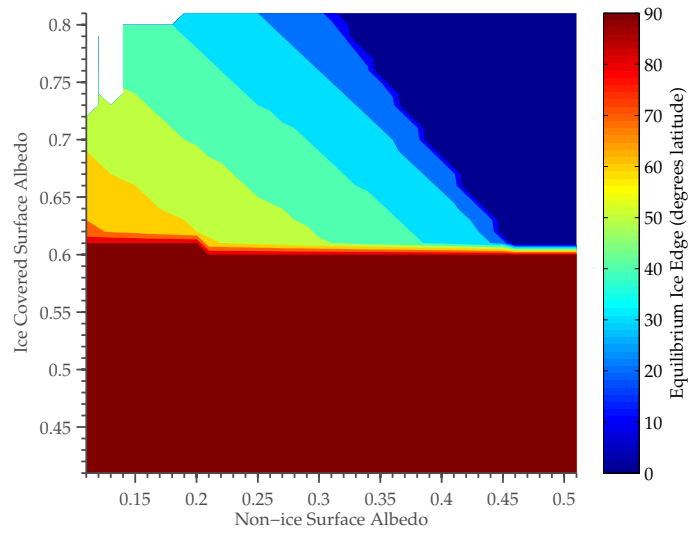
4.3.1   *Results*

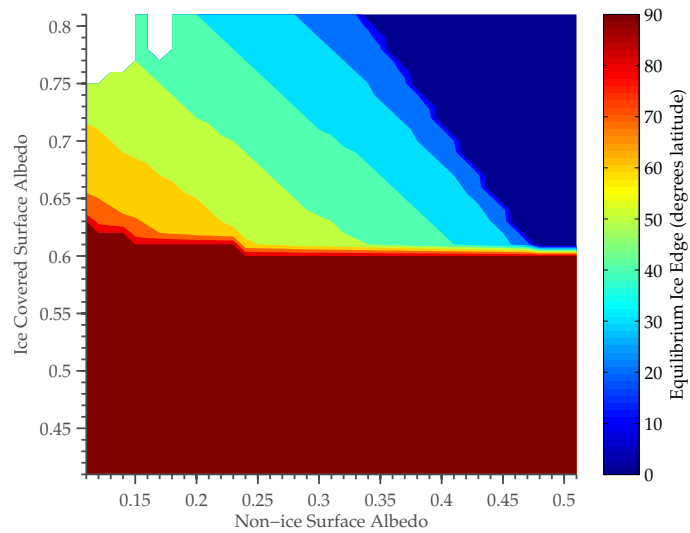Figure 22: 1 Phase model sensitivity to albedo value.

Figure 23: 3 Phase model ice edge sensitivity to albedo value. Colours denote equilibrium ice edge position.

Figures 22 and 23 show the equilibrium ice edge for all permutations of ice and non-ice albedo used in the study. Blank areas in the contour map are permutations that failed to converge to an equilibrium ice edge. This occurred where ice albedo was much higher than non-ice albedo, which caused temperature differentials at the ice edge to be high enough that the differential equation solver diverged between time steps, causing a runaway divergence in the solution. The results are very similar for 1 and 3 phase models, but with the 1 phase model having a slightly larger proportion of snowball earth states.This effect is probably due to the increased sensitivity to albedo in the 1 phase model, which in turn is due to the 1 phase model having a greater proportion of radiation reaching the surface (due to a lack of cloud to reflect it). This effect is described in Section 4.1.2. The general similarity between models is probably due to model tuning removing differences between the variants, and thus we focus just on the single phase model in the remainder of our discussion. For ice albedos below 0.6, only ice-free states occurred. This is a side-effect of the calibration process - an approximate 72 degree equilibrium ice edge is very close to the size of the small ice edge instability, and so ice edges greater than this tend to be only quasi-stable, settling into an ice-free state eventually. This highlights the importance of running the model for a sufficient number of steps in order to be confident the results are correct for cases near state transitions.

Figure 24 shows all permutation of ice and non-ice albedo as a differential, A:

$$A = |r_{s,ice} - r_{s,non-ice}| \tag{44}$$

Each value of A is then plotted against the difference in mean equilibrium temperature between the two layers (surface minus atmosphere).

As the albedo differential increases, the negative gradient for the finite ice edge portion of the plot (all points that are not 0 or 90 inclusive) increases. This means the sensitivity to changes increases as albedo differential increases, which effectively is changing the magnitude of the surface ice feedback. This is evidenced by the fact the greatest albedo differentials (> 0.8) only appear at either 0 or 90 degrees equilibrium ice edge - for these differentials, the model is too sensitive to exist in the finite ice edge state at all.
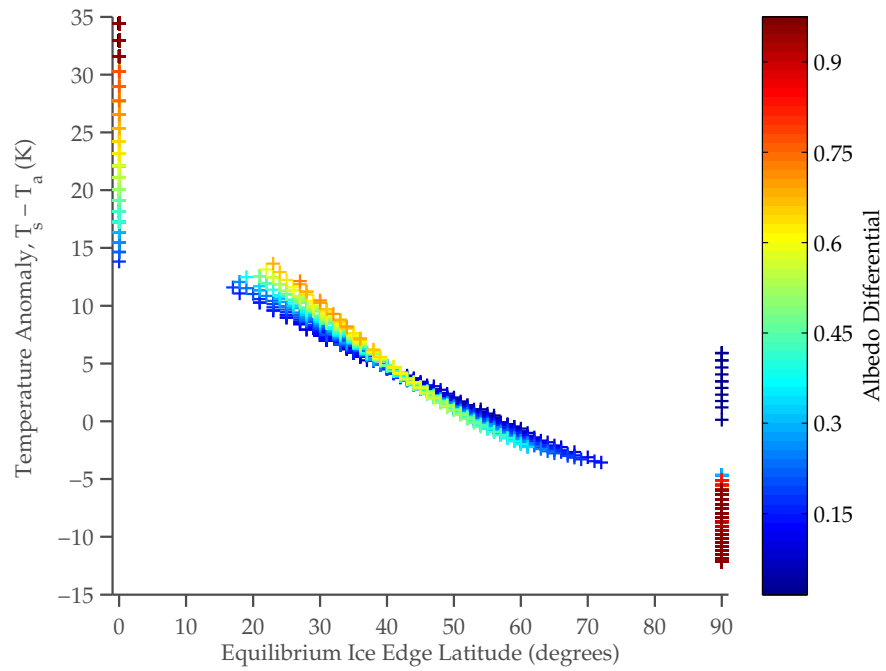
Figure 24: Ice edge equilibrium positions for all permutaions of albedo differential.

Extending from Figure 24, Figure 25 shows the percentage of each solution state the model equilibriated into for any given albedo differential (each differential could represent many different permutations of ice and non-ice albedo). Again, higher differentials lead to less finite ice states (representing a loss in stability). Figure 25 also shows that for high enough albedo differentials, the proportion of snowball states also decreases. The reason for this is that while high non-ice/low ice differentials end in ice free states, higher ice/lower non-ice simply fail to converge. Higher non-ice/lower ice differentials are effectively showing how an EBM with little/no ice feedback behaves because the low ice albedo means the surface ice feedback is greatly reduced. This means that absorption on the surface greatly outweighs any reflection from albedo, which in turn causes most models at this end of the sensitivity study to equilibriate in the ice free state.

To further demonstrate the effect of removing ice feedback, a sensitivity run was conducted where ice albedo and non-ice albedo were given the same value of 0.3, effectively removing the ice feedback effect. Figure 26 shows the components of heat flux between layers in the system (using the same technique as Figures 17 and 18). All components of flux can be seen to have a slightly non-linear upward gradient, with surface layer emitted longwave and absorbed shortwave
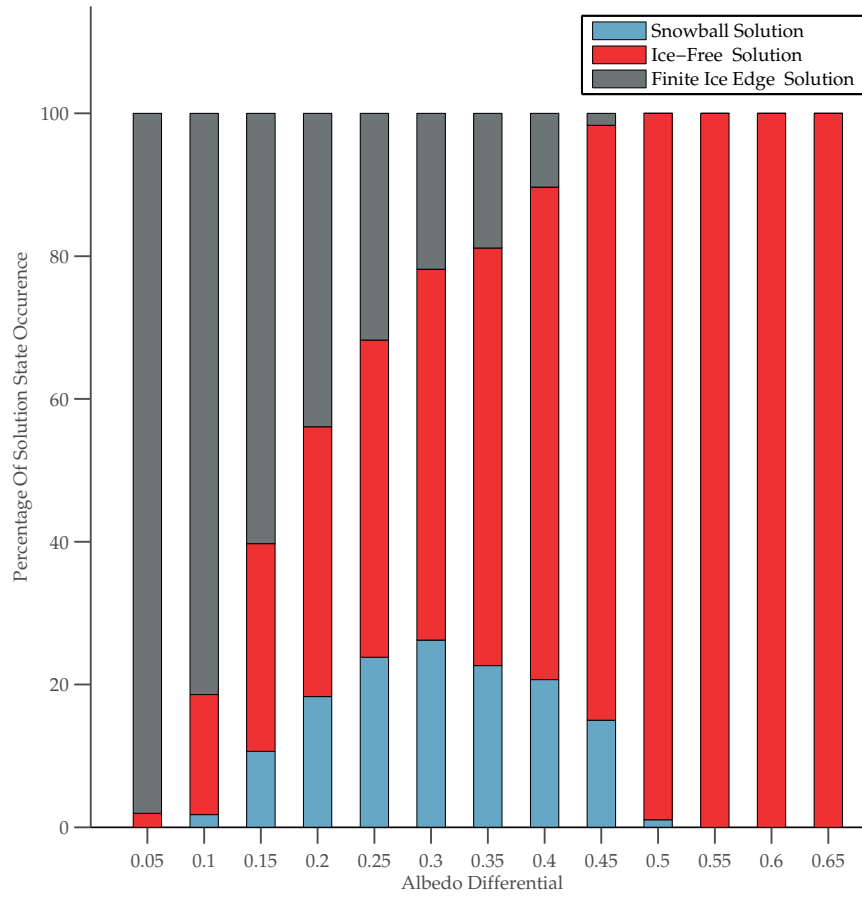
Figure 25: Percentage of equilibrium states for albedo differential.

showing the greatest sensitivity to increase of S_0. This shows why large differentials in albedo produce ice-free solutions - these components of flux in the model dominate the others. Figure 27 shows the corresponding changes in cloud fraction distribution with respect to increasing values of S_0 for this sensitivity run. The pattern is the same unrealistic result as seen in Figure 16.

The result that changing the albedo of surface ice affects the stability of the climate system has implications for the current state of the climate. For example, recent research suggests that anthropogenic black carbon (soot) has a much larger effect on radiation forcing than was previously known [7], and black carbon also plays a significant role in modification of surface albedo especially in Arctic latitudes, by darkening snow and ice [47]. The albedo sensitivity results suggest that black carbon could therefore have larger broad effects on the state of the climate.
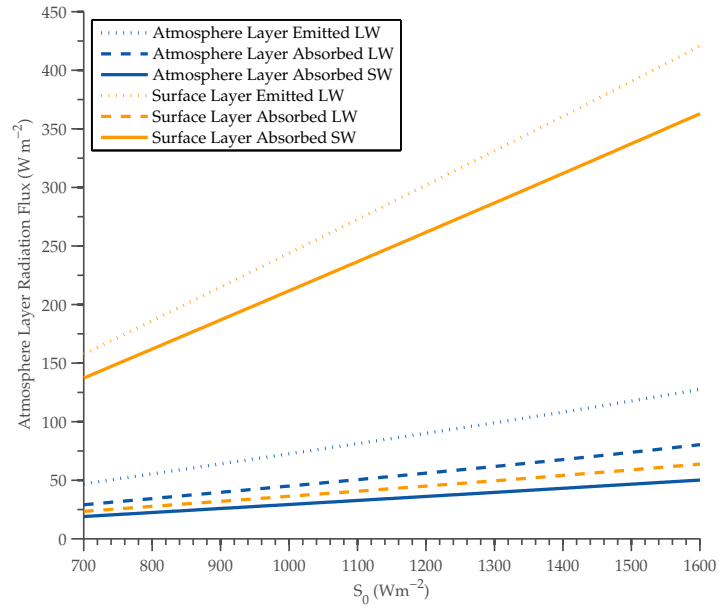
Figure 26: Components of energy flux for a model sensitivity run with no ice feedback.
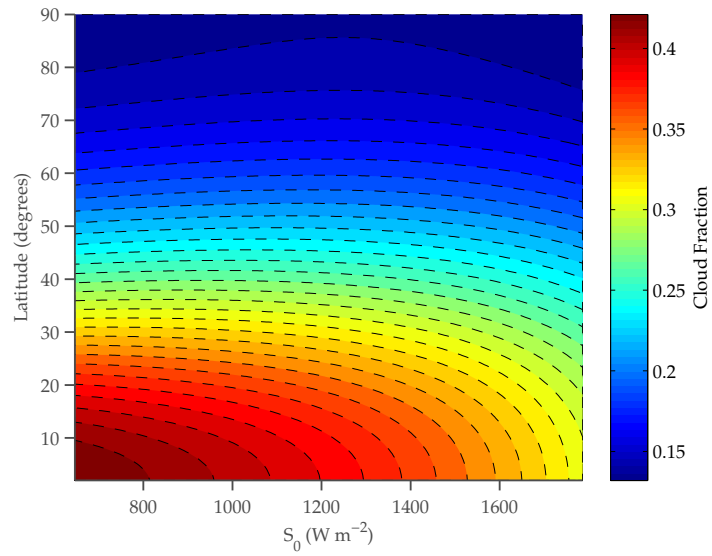

Figure 27: Distribution of cloud fraction for a model sensitivity run with no ice feedback.

4.4 RELATIVE HUMIDITY SENSITIVITY
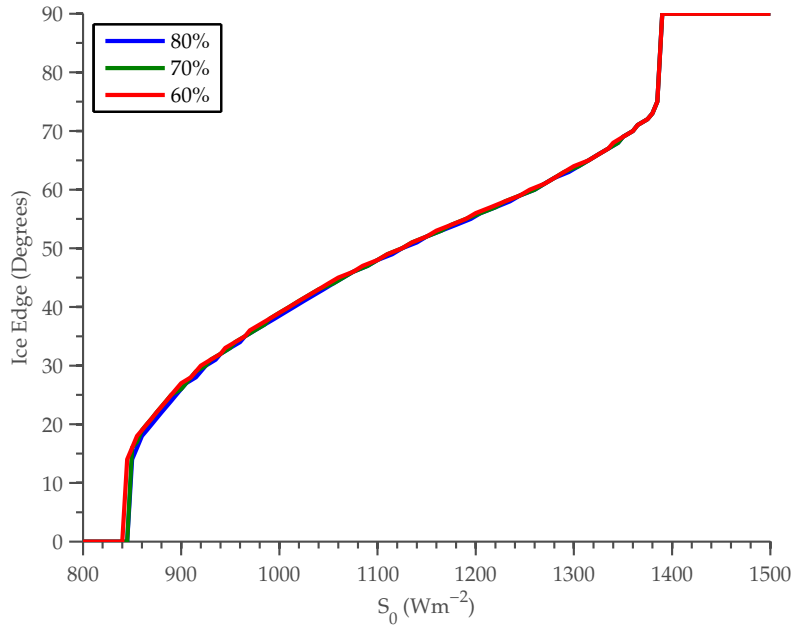
Figure 28: Sensitivity of model to Relative humidity of surface layer.

The prognostic variable that was varied in this study was *RH*, the relative humidity of the surface layer. As mentioned in the introduction to this chapter, relative humidity was chosen as it is a good metric for water vapour feedback, as it affects the amount of water vapour on the surface (Equation 25 in Section 3.2.1.3), which in turn affects the amount of water vapour in the atmosphere.

4.4.1 *Results*

Figure 28 clearly shows that the model was insensitive to changes in this variable. This is explained by the moisture under-estimation effect explained in Section 4.5.

4.5   WATER VAPOUR UNDERESTIMATION

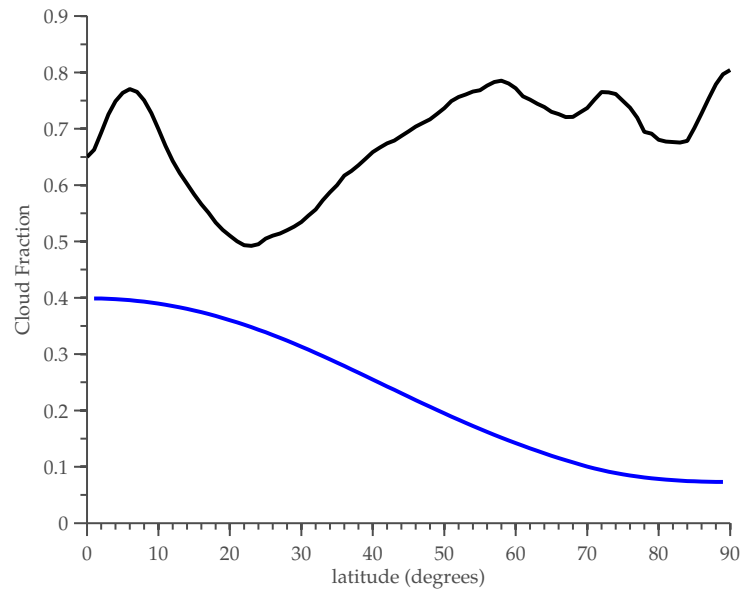Figure 29: Mean annual cloud fraction by latitude for northern hemisphere from MODIS Combined satellite data (black), compared to $1366\,\mathrm{Wm}^{-2}$ 3 phase model run equilibrium cloud fraction (Source: NASA Land Processes Distributed Active Archive Center (LP DAAC). MOD08 M3. USGS/Earth Resources Observation and Science (EROS) Center, Sioux Falls, South Dakota. 2003-2009).

As observed in this chapter (especially in Figure 12), the addition of water vapour alone has very little effect on the sensitivity of the system. This was due to a systematic underestimate in the magnitude of water vapour available in the system for both 2 and 3 phase variants. This in turn had an effect on the cloud fraction, which for the 3 phase model was approximately half the value found using the annual mean of the MODIS combined cloud fraction product (Figure 29). Note that the larger difference near the poles is not as significant as it appears, as polar region cloud tends to actually have a net heating effect in contrast to cloud in lower latitudes that has a net cooling effect [56].

An attempt was made to force the water vapour to realistic values, but it caused instabilities in the model that could not be corrected for, and so the model failed to converge for the values and ranges used sensitivity studies in this chapter. Thus, we had to work around this problem. Suggestions for ways to correct this issue are also identified in Section 6.1.

STABILITY AND HYSTERESIS

Sensitivity studies are limited to viewing the equilibrium response of the model, as the model must be run to a stable state before an accurate observation of the properties of the solved PDEs can be made. Since the model is solved by explicit time stepping (Section 3.6), the state of the model at any time can be observed. This chapter explores the time-dependent behaviour of the model, and also hysteresis phenomena observed. Hysteresis is explained in detail in Section 5.0.1.

5.0.1 *Hysteresis Theory*

Hysteresis indicates the state of a system which depends not only on the values of the parameters of that system, but the history of variation of those parameters, and is only possible for systems with several stable states [45].
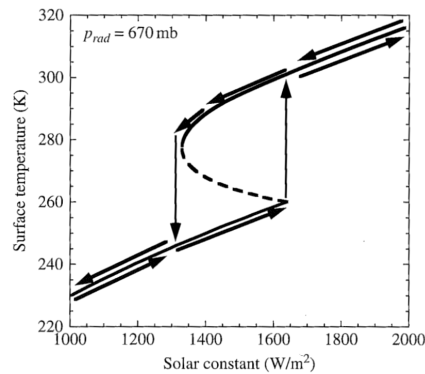

Figure 30: Illustration of the hysteresis effect for an EBM by adjusting the solar constant (Source: [45]). The dotted line represents unstable solutions.

Figure 30 shows an example EBM run, where the solar constant was initially set to $1000\,\mathrm{Wm}^{-2}$, and then was gradually increased to a maximum of $2000\,\mathrm{Wm}^{-2}$, then gradually reduced again to the initial solar constant value. As the solar constant increases, the mean surface temperature also increases. At approximately $1600\,\mathrm{Wm}^{-2}$, the surface temperature is high enough that an ice cap is not possible, the model makes a sudden jump to a higher temperature, and exists in a new ice free state. Running the model further, and by reducing the solar

constant instead of increasing it, the model passes where the state transition occurred while the solar constant was increasing. This is hysteresis. The dotted line represents unstable solutions in the model - runs in that particular range of solar constant will never equilibriate there if the model continues to run. Solutions along the unstable curve are not observed in the EBMs used in this thesis due to conditions on stability detailed in the introduction of Chapter 4.

5.1 TIME EVOLUTION OF MODEL

5.1.1 *Method*

Initial conditions of the model were set using the same values as in Table 4, except that all surface layer latitude zones were initiated with a temperature low enough (255 K) to start with global ice cover. The model was then run to a stable equilibrium with a tuned S_0 value such that the final equilibrium state of the model for $S_0 = 1366 \, \mathrm{Wm}^{-2}$ resulted in the model reaching a final equilibrium position at an ice-free state. This allows the time evolution study to view the model moving through all three stable states possible. The model was initially run as normal with this value of S_0 to confirm that the model converged on a solution, so that the results of the time evolution study can be confirmed as realistic with the Lax-Richtmyer equivalence theorem (explained in Section 3.6).

Samples of temperature for both layers, heat transport in both layers, cloud fraction (for the 3 phase model only), and surface albedo were collected from the model at 1 day intervals. The study was repeated for both 1 and 3 phase models (2 phase model results were similar enough to 1 phase results to be ignored, due to the water vapour underestimation explained in Section 4.5). Each value was recorded for a 0 degree latitude zone (equator), a 45 degree latitude zone (mid-latitude), and a 90 degree latitude zone (pole). Phases and zones used are listed in Table 6.

5.1.2 *Results*

Figures 31 , 32, and 33 show the time evolution of the model for all variables of interest. Figure 31 shows temperature for the surface (left) and atmosphere (right) layers. All temperatures (surface and atmosphere) are initially set to 255K. On the surface, three different temperature trends can be seen. As the run begins, the equatorial zone warms as the other two zones cool. At this point, the entire surface is still ice-covered (the albedo graph on Figure 33 shows that all

MODEL	LATITUDE ZONE	PLOT STYLE
1 Phase	Equator	————————
1 Phase	45 Degrees	– – – – – – – –
1 Phase	Pole	····················
3 Phase	Equator	————————
3 Phase	45 Degrees	– – – – – – – –
3 Phase	Pole	····················

Table 6: Plotting styles for time evolution results.

three zones still have an albedo of 0.6, which is the albedo of ice used in this setup). The warming of the equatorial zone compared to the cooling of the other two zones implies that the equator is receiving more radiation flux than that emitted by a surface at 255 K. Since the temperature is still similar to the other zones, this extra heat is not associated with heat transport (as the heat transport is determined by temperature gradient), so this suggests that the extra insolation the equator zone is receiving (due to the differential insolation curve, as seen in Figure 7) is greater than the loss from ice albedo. At approximately 10^1 days, the equatorial temperature rises above the model T_{crit} (the temperature at which the ice cover in a zone melts), and the gradient of temperature increases rapidly to a significantly greater value, showing that the ice has melted in the equatorial zone, and the albedo has changed to the non-ice value. A similar significant change in gradient is observed at the mid-latitude zone at approximately $10^{1.5}$ days, also due to ice melt. Temperature in the polar zone initially decreases as the emission from the surface outstrips insolation, and then begins to increase (due to increased incoming surface heat transport, seen in the left figure of Figure 32), until reaching T_{crit}, where the gradient becomes nearly vertical.

In the atmosphere layer however, the various changes of the temperature curves observed on the surface are not visible, other than a slight inflection point at 10^1 days, where the surface equatorial zone
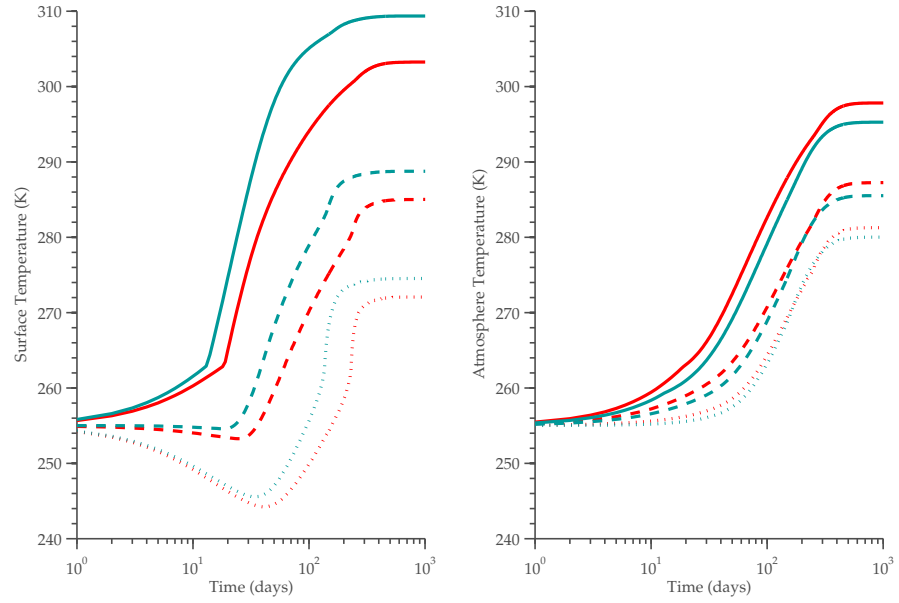
Figure 31: Time evolution of surface and atmosphere layer temperatures.

becomes ice free. This illustrates the fact that while the atmosphere layer is coupled to the surface layer by longwave parameters, this coupling isn't neccessarily strong, and the incoming shortwave and meridional heat transport can play as large or even a larger part in the time evolution of atmosphere layer temperatures. This is surprising when compared to reality, but since the model does not deal with vertical convection or vertical latent heat transport (which can be seen in the global energy balance diagrams of Figure 1), this is understandable.

In all cases, the 1 phase model has greater surface temperatures than the 3 phase model, and lower atmosphere temperatures. This demonstrates the absorbative effect of cloud taking a greater proportion of incoming radiation into the atmosphere layer in the 3 phase model, an effect also observed in the water phase sensitivity study of the model (Section 4.1). This leads to ice melting first in the 1 phase model, which can be observed by the the discontinuity in the equatorial zone surface temperature occuring at 10^1 days in the 1 phase model. The shapes of all temperature curves is largely the same, independent of the model components (1 and 3 phase models). So rather than affecting the character of phenomena in the model, adding positive and negative feedbacks by adding model components is effectively changing the climate sensitivity of the model.

Figure 32 shows the evolution in heat transport for surface (left) and atmosphere (right) layers. Heat transport is a function of temper-
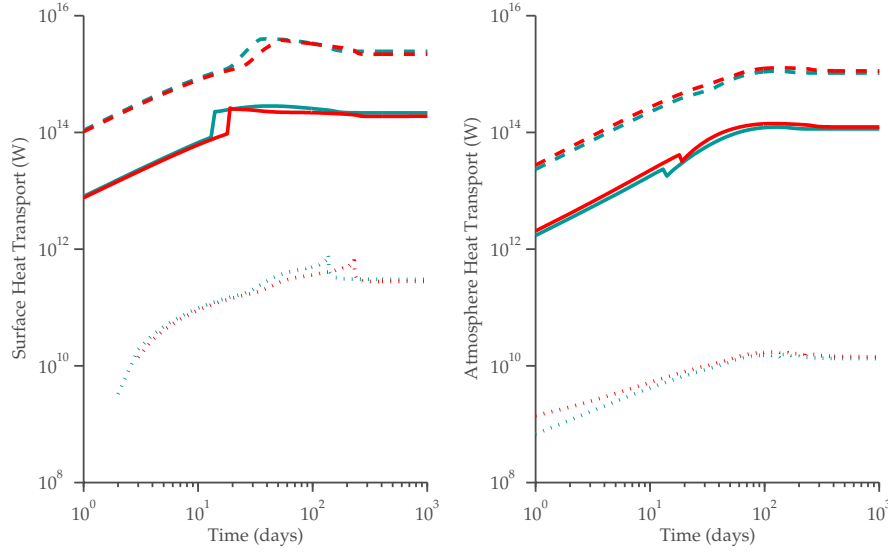
Figure 32: Hysteresis effect comparison between surface heat transport (left) and atmospheric heat transport (right) in 1 and 3 phase models.

ature gradient, and so will maximise around mid latitudes where the temperature gradient is greatest (see Figure 10b). This means the mid latitude zone will always have a greater rate of heat transport than the equator, even though the equator is receiving more heat from insolation. As in Figure 31, the equatorial heat transport jumps at approximately 10^1 days as ice is melted in that zone, producing a rapid change in the temperature gradient. The discontinuity is also visible as a small dip in the atmospheric layer. The pole zone heat transport rate actually decreases after its ice melts. This is due to a decrease in temperature difference between this zone and the zone adjacent, which in turn reduces the heat transport rate. This gradient decrease would be observed in all layers, but at the pole increase in absorbed insolation due to albedo change is lower, as there is less insolation available overall at this latitude.

Figure 33 shows the time evolution of cloud fraction (left) and surface albedo (right). The cloud fraction across all three zones starts at very similar values, as the surface temperatures are uniform at the model start and water vapour availability is defined by the temperature of the latitude zone. After ice melts in the equatorial zone at 10^1 days, cloud fraction at the equator rapidly increases to a level that is close to realistic for that zone, but then decays as the model stays in the finite ice edge space. This phenomenon was replicated in a normal finite ice edge equilibrium 3 phase run (Figure 34), so is not isolated to the ice-covered to ice-free transition used in this study. One possible explanation for this phenomenon is that in creating a
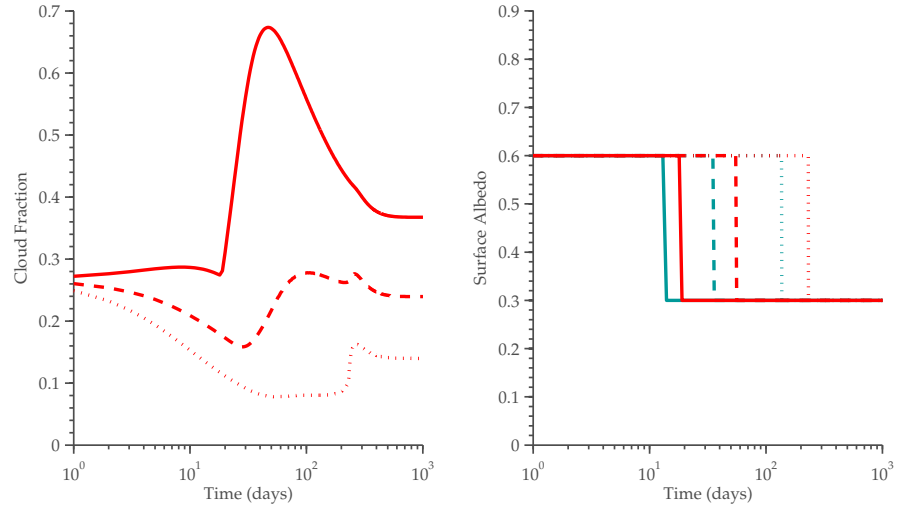
Figure 33: Hysteresis effect comparison of cloud fraction (left) for the 3 phase model only, and surface albedo (right) between 1 and 3 phase models.

significant cloud layer, the atmospheric layer receives a larger proportion of shortwave radiation, which in turn reduces the radiation reaching the surface. This cools the surface, which reduces moisture available to create future cloud. The effect can be seen in Figure 35, which shows the time evolution of longwave and shortwave flux components. A spike in received surface shortwave flux (yellow solid line) is observed at 10 days, which then decays. The shape of the decay reflects the shape of the increase in received atmosphere shortwave flux (blue solid line), suggesting that the surface layer loss is linked to the proportional gain by the atmosphere layer. The differences in magnitude in these two flux shapes can be accounted for by the differences in absorptivity between them, so the shape rather than the magnitude is the important characteristic to observe.

For surface albedo (Figure 33, right), a value of 0.6 indicates the zone is ice covered, and 0.3 indicates the zone is ice free. The albedo plot shows ice melting at the equator first, then the higher latitudes, with the 1 phase model melting before the 3 phase model in all cases, due to the extra insolation the 1 phase model receives.
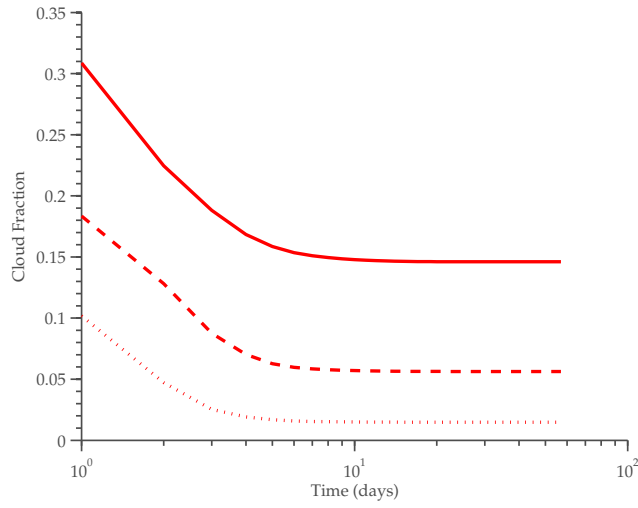
Figure 34: Cloud fraction decay for a 3 phase model run with finite ice edge equilibrium.
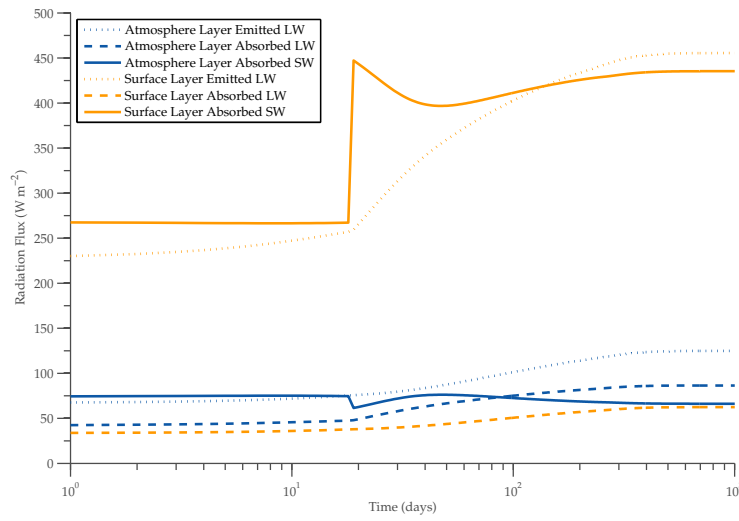
Figure 35: Time evolution of components of longwave and shortwave radiation flux for equator zone.

5.2 HYSTERESIS

5.2.1 *Method*

A single run of the model is conducted with an S_0 value that increases by $10\,\mathrm{Wm}^{-2}$ every 10 days, to some maximum value. At this point the S_0 is reduced by $10\,\mathrm{Wm}^{-2}$ every 10 days until the initial S_0 value is reached. 10 days was chosen as the time interval as it represents the time scale that most state transitions occur over from the sensitivity studies in Chapter 4, and so this time interval allows the model to either equilibriate to some quasi-stable state, or move into a new state before S_0 is changed again. The experiment was also tried with 1 day iterations, but the results were not significantly different.

S_0 was tuned by an amplification factor so that $1366\,\mathrm{Wm}^{-2}$ produced an Earth-like finite ice edge when the model 3 phase variant of the model was run. This tuning was used on both a 1 and 3 phase model, and the two hysteresis runs were compared.

5.2.2 *Results*

Figure 36: Hysteresis effect comparison between 1 and 3 phase models.

Figure 36 shows two hysteresis runs, one for a 1 phase model, and the other for a 3 phase model. Arrows indicate the movement of ice edge over time. The lines are separated into two sections:
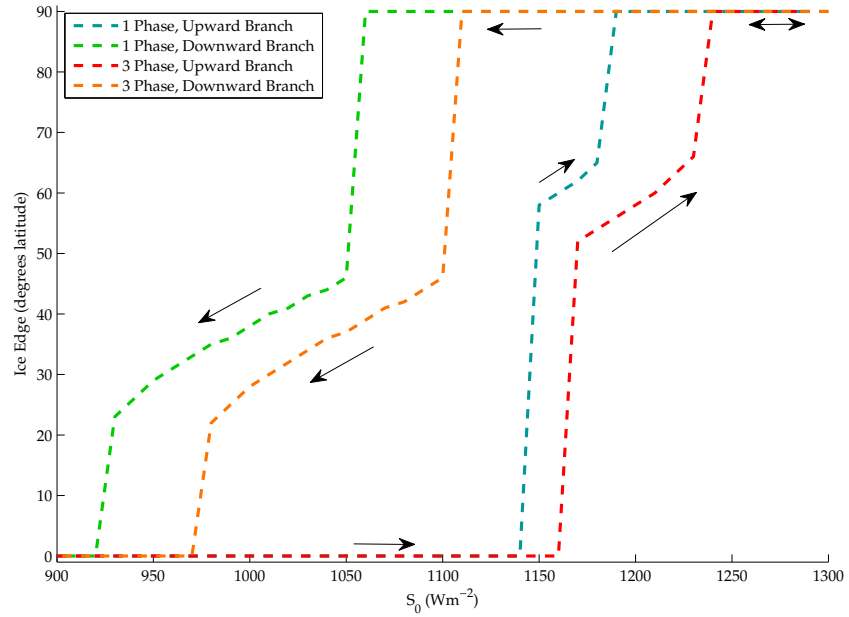
- An "upward branch", representing the ice edge values the model produced while S_0 was increasing.

- A "downward branch", representing the ice edge values the model produced while S_0 was decreasing.

For both runs, a clear hysteresis effect can be observed, as the upward branch does not match the downward path - the ice edge value is dependent on the direction of the change in S_0. Note that at state transitions, the paths appear to have gradients rather than appear vertical as is expected for an instantaneous transition, but this is a simply a side-effect of the S_0 step size in the experiment - a transition in state is from one S_0 step to the next, which is $10\,\mathrm{Wm}^{-2}$ in size. The models are observed to move along the following general path:

1. The models stay at a 0 degree ice edge for some time as S_0 increases, representing a snowball state.

2. At $1140\,\mathrm{Wm}^{-2}$ (for the 1 phase model) and $1160\,\mathrm{Wm}^{-2}$ (3 phase model) the models move to a finite ice edge state.

3. The models exist in a finite ice edge state, with an ice edge that increases as S_0 increases.

4. At an ice edge of 65 degrees latitude (1 phase model) and 66 degrees latitude (3 phase model), the models jump to an ice free state (due to the small ice edge instability).

5. The models move in the ice free state until the maximum S_0 is reached.

6. The value of S_0 is now decreasing, and the models stay in the ice free state for lower S_0 values than they did on the upward branch.

7. At $S_0 = 1060\,\mathrm{Wm}^{-2}$ (for the 1 phase model) and $S_0 = 1110\,\mathrm{Wm}^{-2}$ (3 phase model), the model moves to a finite ice edge state.

8. The models are observed to stay in the finite ice edge state for longer on the downward branch than the upward branch, and achieves a much lower ice edge latitude before the SICI effect causes the model to transition to the snowball state

9. The models run to the minimum S_0 value in the snowball state.

During the finite ice edge states of both the upward and downward branches, the 1 phase model showed a higher ice edge than the 3 phase model for the same S_0 value. This is consistent with the larger insolation the 1 phase model receives for any given value of S_0 - the critical temperature to melt the equatorial ice and begin the finite ice edge state is reached first.

Stability of the models for both upward and downward phases was observed from the size of the range of S_0 values the models were in the finite ice edge state - the greater the S_0 range was in the finite state, the more stable the model was to be considered. On the upward branch, the 1 phase model was in the finite ice edge state for a much smaller range of S_0 values than the 3 phase model, and so was less stable on the upward branch. On the downward branch, the models stayed in the finite ice edge state for relatively similar ranges of S_0, and so were relatively equally stable on the downward branch.

The fact the 1 phase model is more stable on the downward branch isn't easily explainable.
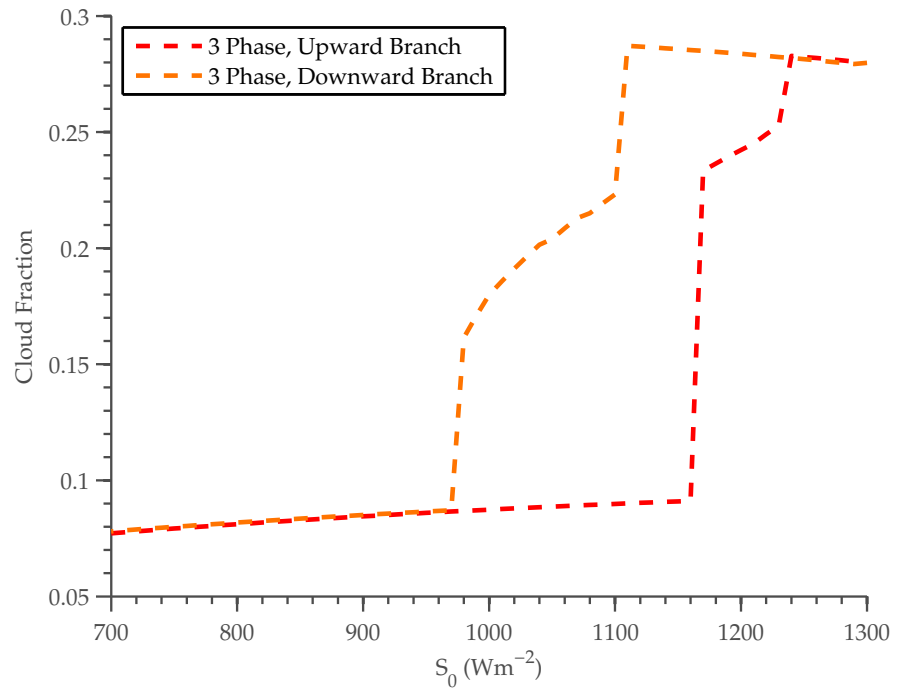
Figure 37: Time evolution of mean cloud fraction in hysteresis study.

Figure 37 shows the evolution of mean cloud fraction for the 3 phase model in the hysteresis experiment. As in Figure 36, the plot is split into two branches, with the upward branch showing cloud fraction as S_0 is increased, and the downward branch showing cloud fraction as S_0 is decreased. Again the upward and downward branches

do not match - the cloud fraction stays higher for lower values of S_0 on the downward branch.

6

CONCLUSION

The aim of the thesis was to use energy balance models to explore the behaviour of and interrelationships between water feedbacks for all phases of water as they exist on earth. A two-layered (suface and atmosphere) Budyko-Sellers [8] [53] style energy balance model was modified with parameterizations for water vapour and cloud in the atmosphere, which could be added or removed in order to conduct experiments.

The additions to the model produced results that were generally physically plausible, with some persistent issues. In particular, the shape and structure of temperatures and heat transports as functions of latitude were comparable to the earlier work of Rose and Marshall [52], but the magnitudes of heat transport were smaller, and the surface layer had a larger peak heat transport than the atmosphere layer, which was the reverse of the Rose and Marshall result and reality. This was probably due to the atmosphere having a smaller meridional temperature gradient than the Rose and Marshall model, which would have restricted heat transport, as heat transport is calculated using it. The water vapour parameter also consistently underestimated the amount of water vapour to produce, which resulted in reduced cloud fraction and reduced water vapour feedback, but the cause for this could not be determined. However, given the simplicity of the parameterizations used, the plausible (if sometimes too small) variations suggest that this model shows promise.

The sensitivity of the model was tested by progressively adding surface ice ("1 phase model"), water vapour ("2 phase model"), and cloud ("3 phase model") feedbacks, and by examining the model's sensitivity to several prognostic variables (atmospheric layer pressure, albedo values, and surface relative humidity). The 1 and 2 phase models produced very similar results, which is likely to be caused by the underestimation of water vapour in the surface layer. For this reason, the relative humidity had little effect on the sensitivity of the model. Comparing 1 and 3 phase models, the addition of cloud was found to change the proportions of heat in the climate system, absorbing a portion of shortwave radiation that would have reached the surface, and reflecting another portion away before it could be absorbed. This changed the ratio of mean heat transport between the layers - the 1 phase model had a ratio of surface transport to atmo-

sphere transport of 2.4953 compared to the 3 phase model ratio of 2.0626 - much more of the total heat transport was occurring in the atmosphere layer for the 3 phase model. Changing the atmospheric layer pressure acted to change to cloud and water vapour feedback strength. Changing albedo values was found to be a good proxy for examining the strength of the surface ice feedback, showing that as the feedback increases, the model spends less time in the finite ice edge state, which represented a loss in stability. Since anthropogenic black carbon affects surface ice and snow albedo in Arctic latitudes, the results suggest that black carbon could have an effect on the stability of the ice cap, which could be explored further in future work.

One of the key questions that was initially considered when developing the EBM was whether the interaction of multiple water-based feedbacks would enhance or diminish polar amplification. Thus, the model was tested for evidence of polar amplification, and showed evidence of the effect for both 1 and 3 phase models, as surface temperatures in the polar latitudes (70-90 degrees latitude) were more sensitive to increasing S_0 than non-polar latitudes (0-70 degrees latitude). The addition of cloud feedback strengthened this effect, which agrees with the results of Graversen and Wang [18] that changes in radiative balance due to the addition of cloud increased the amplification effect.

The time dependent behaviour of the model and its stability was also explored by exploiting the time stepping nature of the FTCS numerical solving method used for the EBM. The model was run from an ice-covered surface to an ice free state for a single value of S_0 for both 1 and 3 phase model variants, and the time evolution of temperatures, heat transport, cloud fraction, and albedo were studied for three latitudes (equatorial, mid-latitude, and polar). The equatorial latitude was observed to heat earlier and to a greater extent due to the increased insolation it received, with larger heat transports due to a larger temperature gradient between zones. Comparing the 1 and 3 phase models, the extra insolation received by the surface layer in the 1 phase model caused it to change states to the finite ice edge state and ice free state in a shorter time than the 3 phase model.

The model was examined for evidence of hysteresis, and this was confirmed for both 1 and 3 phase models. The 1 phase model exhibited less stability during the hysteresis run, which was quantified as the 1 phase model spending a smaller range of S_0 in the finite ice edge state as S_0 was increased.

6.1 FUTURE WORK

Relevant future work on the model would be to improve the parameterization of water vapour to bring amounts in line with empirical values and thus increase the cloud fraction to more realistic values, add new climatic phenomena to the model by developing parameterizations using the same methods as used by this thesis, and explore different methods of solving the partial differential equations that form the base of the model.

A persistent issue with the model was the underestimation of water vapour on the surface layer (Section 4.5), which in turn reduced the cloud fraction as the cloud is generated from available water vapour. This meant that the 2 phase model (with water vapour feedback but no cloud) produced results that were very similar to the 1 phase model. One possible reason for this is the lack of convective transport in the model (as discussed in Section 1.1.3). If a parameterization of convection of water vapour can be added to allow for a greater amount of water vapour to be transported to the atmosphere layer, the cloud fraction could improve. Finally, it is possible that the empirical fit used by Barker [4] to get values for the function that defines γ in the model (Section 39) may not be good enough for the model. Recalculating γ may improve the stability of the model with higher, more realistic levels of water vapour.

One feature of the shape of the cloud fraction curve as a function of latitude that has not been considered is the effect of the Hadley cell. The Hadley cell is a tropical atmospheric circulation which can be observed to affect mean annual cloud fraction by reducing in cloud coverage from 10 to 30 degrees latitude (visible in MODIS data plotted in Figure 29 in Section 4.5). Adding parameters to the cloud fraction in order to account for this regional reduction could produce results of interest. Jentsch's model [29] included a parameterisation of the Hadley cell, this could be used to add the functionality to the model.

Addition of a black carbon parameter would be useful to explore the albedo sensitivity of the model to the darkening effects of black carbon discussed in Section 4.3.1, to see to what extent black carbon affects the overall stability of the model - whether the small ice edge instability becomes more or less pronounced, and for what range the model stays in the finite ice edge state.

The Crank-Nicolson method for solving the partial differential equations in the model was rejected due to persistent oscillations in the solution, but it is possible that with the addition of well-justified damping parameters, this oscillation could be reduced or eliminated. The Crank-Nicolson method is considered to be a more accurate method

for solving parabolic PDEs than the FTCS method used, and so may be a good future direction to consider. The Crank-Nicolson method may allow the model to converge to a solution where FTCS did not, and in particular using realistic amount of water vapour (which failed to converge with FTCS) may work with this method.

[1] OA Alduchov and RE Eskridge. Improved Magnus form approximation of saturation vapor pressure. *Journal of Applied Meteorology*, 1996. URL http://journals.ametsoc.org/doi/abs/10.1175/1520-0450(1996)035%3C0601:IMFAOS%3E2.0.CO%3B2.

[2] Vladimir a. Alexeev and Craig H. Jackson. Polar amplification: is atmospheric heat transport important? *Climate Dynamics*, 41(2):533–547, December 2012. ISSN 0930-7575. doi: 10.1007/s00382-012-1601-z. URL http://link.springer.com/10.1007/s00382-012-1601-z.

[3] K. Bar-Eli and Richard J. Field. Earth-average temperature: A time delay approach. *Journal of Geophysical Research*, 103 (D20):25949, October 1998. ISSN 0148-0227. doi: 10.1029/98JD02273. URL http://www.agu.org/pubs/crossref/1998/98JD02273.shtml.

[4] John R. Barker. An introduction to global warming. *American Journal of Physics*, 67(12):1216, December 1999. ISSN 00029505. doi: 10.1119/1.19108. URL http://link.aip.org/link/?AJP/67/1216/1&Agg=doi.

[5] J Bendtsen. Climate sensitivity to changes in solar insolation in a simple coupled climate model. *Climate dynamics*, pages 595–609, 2002. doi: 10.1007/s00382-001-0198-4. URL http://www.springerlink.com/index/LKD2KUT82WHHL93D.pdf.

[6] Craig F. Bohren and Eugene E. Clothiaux. *Fundamentals of Atmospheric Radiation*. John Wiley & Sons, 2006. ISBN 3527608370. URL http://books.google.com/books?id=XomQ4Qyyyy8C&pgis=1.

[7] Tami C Bond, Sarah J Doherty, DW Fahey, PM Forster, T Berntsen, BJ DeAngelo, MG Flanner, S Ghan, B Kärcher, Dorothy Koch, et al. Bounding the role of black carbon in the climate system: A scientific assessment. *Journal of Geophysical Research: Atmospheres*, 118(11):5380–5552, 2013.

[8] MI Budyko. The effect of solar radiation variations on the climate of the earth. *Tellus*, 7, 1969. URL http://onlinelibrary.wiley.com/doi/10.1111/j.2153-3490.1969.tb00466.x/abstract.

[9] RF Cahalan and GR North. A stability theorem for energy-balance climate models. *Journal of Atmospheric Sciences*. URL http://adsabs.harvard.edu/abs/1979JAtS...36.1178C.

[10] Robert J Charlson, Francisco P J Valero, and John H Seinfeld. Atmospheric science. In search of balance. *Science (New York, N.Y.)*, 308(5723):806–7, May 2005. ISSN 1095-9203. doi: 10.1126/science. 1108162. URL http://www.ncbi.nlm.nih.gov/pubmed/15879202.

[11] TJ Crowley, WT Hyde, and WR Peltier. CO2 levels required for deglaciation of a "near-snowball" Earth. *Geophysical Research . . .*, (2), 2001. URL http://onlinelibrary.wiley.com/doi/10.1029/2000GL011836/full.

[12] WH Dines. The heat balance of the atmosphere. *Quarterly Journal of the Royal Meteorological Society*, 43(182):151–158, 1917.

[13] Dietmar Dommenget and Janine Flöter. Conceptual understanding of climate change with a globally resolved energy balance model. *Climate Dynamics*, 37(11-12):2143–2165, March 2011. ISSN 0930-7575. doi: 10.1007/s00382-011-1026-0. URL http://www.springerlink.com/index/10.1007/s00382-011-1026-0.

[14] Kerry Emanuel. A simple model of multiple climate regimes. *Journal of Geophysical Research*, 107(D9):4077, 2002. ISSN 0148-0227. doi: 10.1029/2001JD001002. URL http://www.agu.org/pubs/crossref/2002/2001JD001002.shtml.

[15] I. J. Fairchild and M. J. Kennedy. Neoproterozoic glaciation in the Earth System. *Journal of the Geological Society*, 164 (5):895–921, September 2007. ISSN 0016-7649. doi: 10.1144/0016-76492006-191. URL http://jgs.lyellcollection.org/cgi/doi/10.1144/0016-76492006-191.

[16] Stanley J. Farlow. *Partial Differential Equations for Scientists and Engineers*. John Wiley & Sons, Incorporated, 1983. ISBN 047188698X. URL http://books.google.com/books?id=gHuqPwAACAAJ&pgis=1.

[17] Jean-Baptiste Joseph Fourier. On the Temperatures of the Terrestrial Sphere and Interplanetary Space. *M'emoires d l'Academie Royale des Sciences de l'Institute de France*, 7:570–604, 1827. URL http://books.google.com/books?hl=en&lr=&id=lhzK1-woaiQC&oi=fnd&pg=PA7&dq=On+The+Temperatures+of+the+Terrestrial+Sphere+and+Interplanetary+Space&ots=Ok5MXfmZVn&sig=l63bw8_IHL2mPYjApO2l7pw2jVQ.

[18] Rune Grand Graversen and Minghuai Wang. Polar amplification in a coupled climate model with locked albedo. *Climate Dynamics*, 33(5):629–643, February 2009. ISSN 0930-7575. doi: 10.1007/s00382-009-0535-6. URL http://link.springer.com/10.1007/s00382-009-0535-6.

[19] Charles E. Graves, Wan-Ho Lee, and Gerald R. North. New parameterizations and sensitivities for simple climate models. *Journal of Geophysical Research*, 98(D3):5025, 1993. ISSN 0148-0227. doi: 10.1029/92JD02666. URL http://doi.wiley.com/10.1029/92JD02666.

[20] J. Hansen. Efficacy of climate forcings. *Journal of Geophysical Research*, 110(D18):D18104, 2005. ISSN 0148-0227. doi: 10.1029/2005JD005776. URL http://www.agu.org/pubs/crossref/2005/2005JD005776.shtml.

[21] Dennis L. Hartmann. *Global Physical Climatology*. Academic Press, 1994. ISBN 0080571638. URL http://books.google.com/books?id=Zi1coMyhlHoC&pgis=1.

[22] DL Hartmann and DA Short. On the Role of Zonal Asymmetries in Climate Change. *Journal of Atmospheric Sciences*, 1979. URL http://adsabs.harvard.edu/abs/1979JAtS...36..519H.

[23] Isaac M Held and Brian J Soden. Water vapor feedback and global warming. *Annual review of energy and the environment*, 25(1):441–475, 2000.

[24] Isaac M. Held and Max J. Suarez. Simple albedo feedback models of the icecaps. *Tellus A*, December 1974. ISSN 1600-0870. doi: 10.3402/tellusa.v26i6.9870. URL http://journals.sfu.ca/coaction/index.php/tellusa/article/view/9870.

[25] MI Hoffert, AJ Callegari, and CT Hsieh. The Role of Deep Sea Heat Storage in the Secular Response to Climatic Forcing. *J. Geophys. Res*, 85(Cll):6667–6679, 1980. URL http://www.climatesci.org/publications/pdf/hoffert.pdf.

[26] P. F. Hoffman. A Neoproterozoic Snowball Earth. *Science*, 281(5381):1342–1346, August 1998. doi: 10.1126/science.281.5381.1342. URL http://www.sciencemag.org/cgi/doi/10.1126/science.281.5381.1342.

[27] Takashi Ikeda and Eiichi Tajika. A study of the energy balance climate model with CO2-dependent outgoing radiation: Implication for the glaciation during the Cenozoic. *Geophysical research*

letters, 26(3):349–352, 1999. URL http://onlinelibrary.wiley.com/doi/10.1029/1998GL900298/full.

[28] D Jacob, BJJM Van den Hurk, U Andrae, G Elgered, C Fortelius, LP Graham, SD Jackson, U Karstens, Chr Koépken, R Lindau, et al. A comprehensive model inter-comparison study investigating the water budget during the baltex-pidcap period. *Meteorology and Atmospheric Physics*, 77(1-4):19–43, 2001.

[29] Volker Jentsch. An Energy Balance Climate Model With Hydrological Cycle 1. Model Description and Sensitivity to Internal Parameters. *Journal of Geophysical Research: Atmospheres*, 96(D9): 17169 – 17179, 1991.

[30] Volker Jentsch. An energy balance climate model with hydrological cycle: 2. Stability and sensitivity to external forcing. *Journal of Geophysical Research*, 96(D9):17181, 1991. ISSN 0148-0227. doi: 10.1029/91JD01477. URL http://doi.wiley.com/10.1029/91JD01477.

[31] J. T. Kiehl and Kevin E. Trenberth. Earth's Annual Global Mean Energy Budget. *Bulletin of the American Meteorological Society*, 78(2):197–208, February 1997. ISSN 0003-0007. doi: 10.1175/1520-0477(1997)078<0197:EAGMEB>2.0.CO;2. URL http://journals.ametsoc.org/doi/abs/10.1175/1520-0477%281997%29078%3C0197%3AEAGMEB%3E2.0.CO%3B2.

[32] AA Lacis and J Hansen. A parameterization for the absorption of solar radiation in the earth's atmosphere. *Journal of the Atmospheric Sciences*, 1974. URL http://journals.ametsoc.org/doi/abs/10.1175/1520-0469(1974)031%3C0118:APFTAO%3E2.0.CO;2.

[33] WH Lee and GR North. Small ice cap instability in the presence of fluctuations. *Climate dynamics*, 246:242–246, 1995. URL http://link.springer.com/article/10.1007/BF00215010.

[34] Beate G Liepert and Michael Previdi. Inter-model variability and biases of the global water cycle in CMIP3 coupled climate models. *Environmental Research Letters*, 7(1):014006, March 2012. ISSN 1748-9326. doi: 10.1088/1748-9326/7/1/014006. URL http://stacks.iop.org/1748-9326/7/i=1/a=014006?key=crossref.f54570c296a0dca935acc71c39838f58.

[35] RQ Lin and GR North. A study of abrupt climate change in a simple nonlinear climate model. *Climate dynamics*, 261:253–261, 1990. URL http://link.springer.com/article/10.1007/BF00211062.

[36] RS Lindzen and B Farrell. Some realistic modifications of simple climate models. *Journal of the Atmospheric Sciences*, 1977. URL http://journals.ametsoc.org/doi/abs/10.1175/1520-0469(1977)034%3C1487%3ASRMOSC%3E2.0.CO%3B2.

[37] Claussen M., Mysak L., Weaver A., Crucifix M., Fichefet T., Loutre M.-F., Weber S., Alcamo J., Alexeev V., Berger A., Calov R., Ganopolski A., Goosse H., Lohmann G., Lunkeit F., Mokhov I., Petoukhov V., Stone P., and Wang Z. Earth system models of intermediate complexity: closing the gap in the spectrum of climate system models. *Climate Dynamics*, 18(7):579–586, March 2002. ISSN 0930-7575. doi: 10.1007/s00382-001-0200-1. URL http://www.springerlink.com/openurl.asp?genre=article&id=doi:10.1007/s00382-001-0200-1.

[38] John Marshall and R. Alan Plumb. *Atmosphere, Ocean and Climate Dynamics: An Introductory Text*. Academic Press, 2007. ISBN 0080556701. URL http://books.google.co.nz/books/about/Atmosphere_Ocean_and_Climate_Dynamics.html?id=KvJfvYBHiegC&pgis=1.

[39] NASA. Earth fact sheet. http://nssdc.gsfc.nasa.gov/planetary/factsheet/earthfact.html.

[40] G. R. North, J. G. Mengel, and D. a. Short. Simple energy balance model resolving the seasons and the continents: Application to the astronomical theory of the ice ages. *Journal of Geophysical Research*, 88(C11):6576, 1983. ISSN 0148-0227. doi: 10.1029/JC088iC11p06576. URL http://www.agu.org/pubs/crossref/1983/JC088iC11p06576.shtml.

[41] GR North. Analytical solution to a simple climate model with diffusive heat transport. *Journal of the Atmospheric Sciences*, 1975. URL http://journals.ametsoc.org/doi/abs/10.1175/1520-0469(1975)032%3C1301%3AASTASC%3E2.0.CO%3B2.

[42] GR North. The small ice cap instability in diffusive climate models. *Journal of the atmospheric sciences*, 1984. URL http://www.met.tamu.edu/people/faculty/north/pdf/(32)North84b.pdf.

[43] GR North, RF Cahalan, and JA Coakley. Energy balance climate models. *Rev. Geophys. Sp. Phys*, 19(1):91–121, 1981. URL http://geotest.tamu.edu/userfiles/88/energy_balance_climate_models_1981.pdf.

[44] Raymond T Pierrehumbert. The hydrologic cycle in deep-time climate problems. *Nature*, 419(6903):191–8, September 2002.

ISSN 0028-0836. doi: 10.1038/nature01088. URL http://www.ncbi.nlm.nih.gov/pubmed/12226673.

[45] Raymond T. Pierrehumbert. *Principles of Planetary Climate*. Cambridge University Press, 2010. ISBN 1139495062. URL http://books.google.com/books?id=bO_U8f5pVR8C&pgis=1.

[46] V Ramanathan. Radiative transfer within the earth's troposphere and stratosphere: A simplified radiative-convective model. *Journal of the Atmospheric Sciences*, 1976. URL http://journals.ametsoc.org/doi/abs/10.1175/1520-0469(1976)033%3C1330:RTWTET%3E2.0.CO;2.

[47] V. Ramanathan and G. Carmichael. Global and regional climate changes due to black carbon. *Nature Geoscience*, 1(4):221–227, March 2008. ISSN 1752-0894. doi: 10.1038/ngeo156. URL http://www.nature.com/doifinder/10.1038/ngeo156.

[48] V Ramanathan, P J Crutzen, J T Kiehl, and D Rosenfeld. Aerosols, climate, and the hydrological cycle. *Science (New York, N.Y.)*, 294(5549):2119–24, December 2001. ISSN 0036-8075. doi: 10.1126/science.1064034. URL http://www.ncbi.nlm.nih.gov/pubmed/11739947.

[49] Gilles Ramstein, Myriam Khodri, Yannick Donnadieu, Frédéric Fluteau, and Yves Goddéris. Impact of the hydrological cycle on past climate changes: three illustrations at different time scales. *Comptes Rendus Geoscience*, 337(1-2):125–137, January 2005. ISSN 16310713. doi: 10.1016/j.crte.2004.10.016. URL http://linkinghub.elsevier.com/retrieve/pii/S1631071304003062.

[50] John O. Roads and Geoffrey K Vallis. An energy balance model with cloud feedbacks. *Tellus A*, 36A(3):236–250, 1984.

[51] BEJ Rose. *Oceanic control of the sea ice edge and multiple equilibria in the climate system*. PhD thesis, 2010. URL http://18.7.29.232/handle/1721.1/62496.

[52] Brian E. J. Rose and John Marshall. Ocean Heat Transport, Sea Ice, and Multiple Climate States: Insights from Energy Balance Models. *Journal of the Atmospheric Sciences*, 66 (9):2828–2843, September 2009. ISSN 0022-4928. doi: 10.1175/2009JAS3039.1. URL http://journals.ametsoc.org/doi/abs/10.1175/2009JAS3039.1.

[53] WD Sellers. A global climatic model based on the energy balance of the earth-atmosphere system. *Journal of Applied Meteorology*, 8:392–400, 1969. URL http:

//books.google.com/books?hl=en&lr=&id=lhzK1-woaiQC&oi=
fnd&pg=PA125&dq=A+global+climatic+model+based+on+the+
energy+balance+of+the+Earth-atmosphere+system&ots=
Ok5LUfk_0o&sig=DKEocW_Y9ZipemImXtpPitDZQcs.

[54] Graeme L. Stephens, Juilin Li, Martin Wild, Carol Anne Clayson,
Norman Loeb, Seiji Kato, Tristan L'Ecuyer, Paul W. Stackhouse,
Matthew Lebsock, and Timothy Andrews. An update on Earth's
energy balance in light of the latest global observations. *Nature
Geoscience*, 5(10):691–696, September 2012. ISSN 1752-0894. doi:
10.1038/ngeo1580. URL http://www.nature.com/doifinder/10.
1038/ngeo1580.

[55] John Strikwerda. *Finite Difference Schemes and Partial Differential
Equations*. SIAM, 2007. ISBN 089871639X. URL http://books.
google.com/books?id=rutC8UwjNVgC&pgis=1.

[56] Patrick C. Taylor, Ming Cai, Aixue Hu, Jerry Meehl, Warren
Washington, and Guang J. Zhang. A Decomposition of Feedback
Contributions to Polar Warming Amplification. *Journal of Cli-
mate*, 26(18):7023–7043, September 2013. ISSN 0894-8755. doi: 10.
1175/JCLI-D-12-00696.1. URL http://journals.ametsoc.org/
doi/abs/10.1175/JCLI-D-12-00696.1.

[57] KE Trenberth and JM Caron. Estimates of merid-
ional atmosphere and ocean heat transports. *Jour-
nal of Climate*, pages 3433–3444, 2001. URL
http://search.ebscohost.com/login.aspx?direct=
true&profile=ehost&scope=site&authtype=crawler&jrnl=
08948755&AN=5856189&h=cJmxXmTML%2FeuVuItRS8Sj0%2FKVt%
2FGfPeu50fYCC3OIPsI1Yz6lo7OCRS6kEW1hyWmwsOonBfAh5jHmZMEwIV55Q%
3D%3D&crl=c.

[58] Zhaomin Wang, Rong-Ming Hu, Lawrence a. Mysak, Jean-Pierre
Blanchet, and Jian Feng. A parametrization of solar energy
disposition in the climate system. *Atmosphere-Ocean*, 42(2):113–
125, June 2004. ISSN 0705-5900. doi: 10.3137/ao.420203. URL
http://www.tandfonline.com/doi/abs/10.3137/ao.420203.

[59] SG Warren and SH Schneider. Seasonal Simulation as a Test
for Uncertainties in the Parameterizations of a Budyko-Sellers
Zonal Climate Model. *Journal of Atmospheric Sciences*, 1979. URL
http://adsabs.harvard.edu/abs/1979JAtS...36.1377W.